Dalton Transactions

Accepted Manuscript

ROYAL SOCIETY OF CHEMISTRY

www.rsc.org/dalton

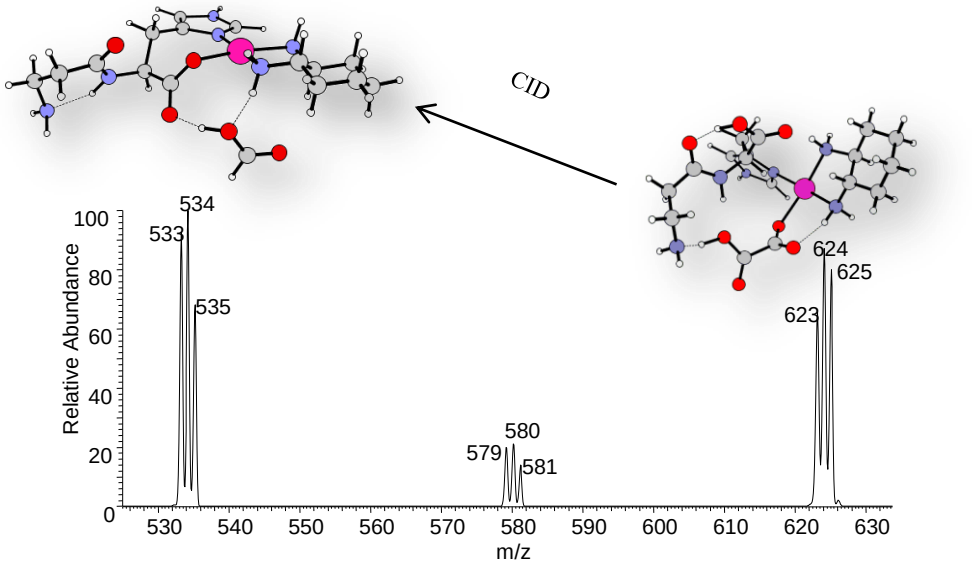

Fragmentation Pathways Analysis for the Gas Phase Dissociation of Protonated Carnosine-Oxaliplatin Complexes.

Ida Ritacco,[a] Eslam M. Moustafa,[b] Emilia Sicilia,[a] Nino Russo[a] and Tamer Shoeib[b][c]*

[a]Dipartimento di Chimica UniVersita della Calabria, Via P. Bucci, cubo 14c, 87036 ArcaVacata di Rende (CS), Centro di Calcolo ad Alte Prestazioni per Elaborazioni Parallele e Distribuite - Centro d'Eccellenza MIUR, Rende 87036, Italy.

[b]Department of Chemistry, The American University in Cairo, New Cairo 11835, Egypt.

[c]Centre for Analytical Science, Department of Chemistry, Loughborough University, Loughborough, Leicestershire LE11 3TU, UK.

* T.Shoeib@aucegypt.edu

Abstract

Collision-induced dissociation (CID) experiments on the protonated carnosine-oxaliplatin complex, [Carnosine + OxPt + H]$^+$ using several collision energies were shown to yield nine different fragment ions. Energy-resolved CID experiments on [Carnosine + OxPt + H]$^+$ showed that the generation of the product ion [Carnosine – H + Pt(dach)]$^+$ (where dach is 1,2-diaminocyclohexane) is the lowest energy process. At slightly higher collision energies the loss of neutral carnosine from [Carnosine + OxPt + H]$^+$ to produce [OxPt + H]$^+$ was observed followed by the loss of oxaliplatin from the same precursor ion to produce [Carnosine + H]$^+$. At significantly higher energies, the ion [OxPt – CO_2 + H]$^+$ was shown to be initially formed while the last two investigated ions [Carnosine + OxPt – CO_2 + H]$^+$ and [Carnosine – NH_3 – H +Pt(dach)]$^+$ were shown not attain any significant relative abundance. Density functional calculations at the B3LYP/LANL2DZ level were employed to probe fragmentation mechanisms that account for all experimental data. The lowest free energy barriers for the generation of each of the ions [Carnosine – H + Pt(dach)]$^+$, [OxPt + H]$^+$, [Carnosine + H]$^+$, [Carnosine + OxPt – CO_2 + H]$^+$ and [Carnosine – NH_3 – H +Pt(dach)]$^+$ from [Carnosine + OxPt + H]$^+$ according to the fragmentation mechanisms offered here were calculated to be 31.9, 38.8, 49.3, 75.2, 85.6 kcal mol^{-1}, respectively.

Introduction

The endogenous dipeptide L-carnosine (β-alanyl-L-histidine)[1-3] is found in different body organs such as the stomach, kidney and at elevated levels in skeletal and cardiac muscles as well as in brain tissue in olfactory bulb and hippocampus.[4,5] Owing to its water solubility, carnosine levels are found to be particularly elevated in cytosolic cellular fractions.[6] Since its discovery there have been many investigations of its biological functions. It is now known, for example, that carnosine is able to interact with aldehydes generated inside the body as a result of glycation reactions which occur between reducing sugar and different body proteins.[7-9] This helps in protecting body proteins, giving carnosine its anti-glycating effect[7-9] which in turn can help in minimizing the effects of some diseases such as diabetes and Alzheimer.[10] Carnosine also has significant anti-inflammatory, antihypertensive, anti-aging, neurological and wound healing effects[11] in addition to possessing unique antioxidant properties due to its ability to interact with highly reactive species, such as hydroxyl, super oxide and molecular oxygen free radicals, especially in the water rich environment inside the body. These antioxidant properties are prominent in the ability of carnosine to hinder lipid peroxidation, which helps in preserving the integrity of body membranes. Carnosine is also known for its buffering capability, being able to buffer the increased acidity generated by lactic acid formation inside muscle tissue during muscle stress.[12] It is also reported that carnosine can act as an effective heavy metal ion chelator able to interact with the circulating metals ions within the body such as iron, calcium, metal containing enzymes and especially copper and zinc.[13] These metal chelating properties make carnosine an effective agent in the prevention and partial reversal of cataracts[14] and in the treatment of Wilsons disease[15] and Alzheimers. The ability of carnosine to bind Zn^{2+} has been found to help modulating neuronal excitability by preventing the Zn^{2+} inhibition of neurotransmitter receptors.[16] In

fact polaprezinc, a commercially available carnosine-zinc(II) drug complex is marketed for its effective antiulcer properties and the ability to improve gastric health.[17-19]

Additionally, it has been shown that carnosine acts as a neuroprotector[20, 21] and can retard tumour growth in mouse models.[22] More recently, it has been reported that carnosine can prevent cell proliferation in colon cancer cells.[23, 24] However, very recently it has been shown that carnosine may be involved in complexation with and sequestering of platinum anti-cancer drugs. Specifically *in vitro* studies on hepatocellular carcinoma HepG2 cells have shown that carnosine may inhibit the cytotoxic action of the third generation chemotherapeutic drug, oxaliplatin, most likely through the formation of complexes that are less cytotoxic than oxaliplatin alone.[25]

Mass spectrometry has proven to be an invaluable technique in studying the interactions between anticancer platinum containing metallodrugs and biomolecules including DNA, proteins and peptides on a molecular level (for recent reviews see references 26 and 27) This is especially important as understanding these interactions allows for a better informed design of future drugs. Studies of anticancer platinum metallodrugs interactions with DNA have been most prevalent as DNA is considered the ultimate pharmacological target for such drugs.[28-30] However, more recently other targets such as proteins and peptides that often play a role in the toxicological profile of platinum anticancer drugs have been considered. Recent examples include the successful use of Fourier transform ion cyclotron resonance mass spectrometry (FT-ICR-MS) with electron capture detection (ECD) to identify the binding sites of cisplatin to several proteins and peptides.[31] In that study, side chain losses from the charge-reduced platinum species provided characteristic indicators for the localization of the Pt-binding sites to certain amino acid residues.[31] In other studies inductively coupled plasma mass spectrometry (ICP-MS) was employed in studying cisplatin binding to the model protein cytochrome C which is a relatively small and well-characterized

protein [32] as well as to plasma proteins being among the major metabolic pathways of this metallodrug. [33] Coupling capillary electrophoresis to ICP-MS, on the other hand, allowed for examining the interaction of different candidate platinum anticancer drugs with human serum anbumin (HSA) including measurements of the kinetics of binding and the determination of number of drug molecules attached to HSA.[34] A similar study where the identification of products formed upon the binding of cisplatin, carboplatin and oxaliplatin with proteins like β-lactoglobulin, HSA and hemoglobin was examined employed Liquid chromatography electrospray ionization time of flight mass spectrometry (LC-ESI-TOF-MS).[35] Finally, electrospray ionization with tandem mass spectrometry (ESI-MS/MS) was employed to probe structural information and examine dissociation pathways for the main reaction products of cisplatin with several sulphur containing peptides.[36]

Specifically a study on the interactions of oxaliplatin with carnosine as well as two of its derivatives β-alanyl-N-methylhistidine (anserine) and N-acetylcarnosine (NAC) was recently reported employing various mass spectrometric techniques utilizing electrospray ionization and chip nanospray.[25] In that study a detailed characterization of the protonated complexes of oxaliplatin with each of these three dipeptide ligands as well as their collision induced fragments have been presented.[25] In the present paper, an analysis of the potential energy surfaces (PESs) for the gas phase dissociation of the protonated carnosine-oxaliplatin complex is presented. A comparison between the calculated potential energy surfaces of the dissociation process and the energy resolved collision induced dissociation of the protonated carnosine-oxaliplatin complex is also reported.

Instrumentation

A tandem quadrupole mass spectrometer, An Acquity TQ (Waters, MA, USA) equipped with electrospray ionisation interface was used in this work. The instrument was operated in

positive ion mode, with typical values of cone and extractor voltages set to 30, and 3 respectively. The capillary voltage was optimised day to day for maximum signal transmission and spray stability, the optimised range was typically 2200-2500 volts. The de-solvation gas was usually set at a flow of 250 L h^{-1} and a temperature of 150 °C. Argon was used as the collision gas at a typical flow rate of 0.15 ml min^{-1}. Ions sampled from the electrospray suffered many collisions in an attempt to achieve effective thermalization in the lens region, being from the orifice/skimmer to the first r.f. only quadrupole. The bias potential in this lens region was set up to strike a compromise between signal transmission and minimal collisional heating. The precursor ions underwent multiple collisions with argon to produce tandem mass spectra obtained at collision energies in the range 0-25 eV in the lab frame having both Q1 and Q3 operated at unit resolution with typical a dwell time of 25 millisecond per transition.

Reagents

Carnosine, HPLC-grade water and methanol were all purchased from Sigma-Aldrich, UK while oxaliplatin was obtained from Sanofi-Synthelabo Limited, UK.

Computational methods

Geometry optimizations without symmetry constraints as well as frequency calculations for all the reactants, intermediates, products and transition states were performed at the Density Functional level of theory by using the hybrid exchange-correlation B3LYP functional[37-40] as implemented in GAUSSIAN03[41] code. For all the atoms the LANL2DZ[42-44] basis sets were employed. The recent successful use of the LANL2DZ basis set is proved by the calculation of both structural details of gold based drug complexes with cysteine and selenocysteine[45] and geometrical features and thermodynamic properties of Cd^{2+} complexes

with GSH.[46] The same basis set was used to gain insight into the decomposition pathways of photo-activated Pt containing anticancer complexes[47] and to obtain excellent agreement with experimental Raman and IR data of Pt-carboplatin complexes.[48] The use of the B3LYP/LANL2DZ computational protocol in investigating transition metal containing compounds is well established.[49-61] In fact, it was recently used to successfully investigate the structures of the anti-arthritic drug auranofin and its complexes with cysteine;[45] to model CO adsorption on Pt nanoclusters;[62] to obtain structural information and binding energies for the complexation of cis- and trans-$Pt(NH_3)_2Cl^+$ to guanine;[57] to investigate monomeric complexes between cisplatin and glutathione;[63] to obtain excellent agreement with X-ray data for cisplatin analogues[64] and oxaliplatin analogues[65]; as well as to examine the mechanism of Pt and Pd catalysed coupling and cyclopropanation reactions between olefins.[66] Most recently, this level of theory was used to study the interactions of the anti-cancer Pt containing drug oxaliplatin with each of the cytoplasmic thiol containing tripeptide ligands γ-L-glutamyl-L-cysteinyl-glycine (GSH)[67] as well as the biologically active β-alanine-L-histidine dipeptide carnosine.[25] In another recent study this level of theory has been employed to study the binding modes and binding energies of carnosine to various biologically relevant metal cations as well as to some Pt based anticancer drugs. In that study the Pt^{2+} binding energy to carnosine was calculated via seven different levels of theory being B3P86/LANL2DZ, B3PW91/LANL2DZ, B3LYP/SDD, B3P86/SDD, B3PW91/SDD, B3LYP/LANL2DZ//6-31G(d) and M06/SDD//6-311G(d,p). It was determined that all values obtained for Pt^{2+} binding energies with the exception of those obtained using B3P86/SDD exhibited relatively small deviation.[68] In addition, the bond dissociation energy of the Pt^+-CH_2 bond was also calculated at five different levels of theory and results were shown to exhibit very small variations.[68] More importantly, results were all, with the exception of the

value calculated at the B3P86/LANL2DZ level of theory, shown to be within 2.3 kcal mol^{-1} of the experimentally determined value.[68, 69]

For each optimized stationary point vibrational analysis was performed to establish its nature either as a minimum (no imaginary frequency) or a first order saddle point (one imaginary frequency). The vibrational mode associated to the imaginary frequency of each intercepted transition state was shown to correspond to the correct movement of the involved atoms. In addition, the intrinsic reaction coordinate (IRC)[70, 71] method was used to show that each located transition state is properly connected to its respective reactants and products along the imaginary mode of vibration. Calculated total electronic energies, zero-point energies, thermal corrections and entropies for all stationary points are given in Supplementary Tables S1-S4.

Results and discussion

Electrospraying a 2:1 mM solution mixture of carnosine with oxaliplatin in 1:1 (v/v) water-methanol solvent system generated the mass spectra shown and assigned in the top panel of Figure 1. The mass selection and subsequent collision induced dissociation (CID) of the ion $[Carnosine + OxPt + H]^+$ resulted in the MS^2 spectra shown in the bottom panel of Figure 1. Performing the CID experiments on the $[Carnosine + OxPt + H]^+$ containing the three most abundant isotopes of platinum being ^{194}Pt, ^{195}Pt and ^{196}Pt confirms that there is no difference in fragmentation pathways among the three platinum isotopes but most importantly allows for a quick identification of the product ions which contain the platinum metal. The product ions observed as labelled in Figure 1 and their precursor ion $[Carnosine + OxPt + H]^+$ were all previously reported and identified.[25] The energy-resolved CID spectra shown in Figure 2 reveals that $[Carnosine + OxPt + H]^+$ initially loses the elements of HOC_2O_2OH to produce the ion $[Carnosine – H + Pt(dach)]^+$ as the lowest energy process. The neutral species lost in

this case, being the elements of HOC_2O_2OH, may be lost as one molecule or as a combination of CO_2 and HCOOH or CO_2, H_2O and CO. At slightly higher collision energies the loss of neutral carnosine from $[Carnosine + OxPt + H]^+$ to produce $[OxPt + H]^+$ can be observed followed by the loss of oxaliplatin from the same precursor ion to produce $[Carnosine + H]^+$. It is interesting to note that even at the highest collision energies employed here no evidence of declining relative abundances of these three fragment ions were observed, in fact in all the three cases no clear maximum was reached. This implies that subsequent fragmentation reactions of these three product ions, due to tertiary collisions, may be considered to have a minimum contribution to the overall observed fragmentation pattern. At significantly higher energies, however, the ion $[OxPt - CO_2 + H]^+$ is shown to be initially formed, reaching a modest 9% relative abundance while its most likely precursor $[Carnosine + OxPt - CO_2 + H]^+$ as well as the last ion observed $[Carnosine - NH_3 - H + Pt(dach)]^+$ were shown not attain any significant relative abundance.

Fragmentation Mechanism 1

Two mechanisms are presented for the loss of CO_2 from $[carnosine + OxPt + H]^+$, see Figures 3 and 4 as well as Scheme 1. In both mechanisms the initial starting point is the precursor ion $[carnosine + OxPt + H]^+$ in its lowest gas phase conformation, structure 1A as shown in Figures 7-9 and Schemes 1-3. This conformer of protonated carnosine-oxaliplatin complex was previously shown to be the global minimum on this potential energy surface.[25] Structure 1A involves Pt coordination to the *pros* nitrogen atom of the histidine ring of carnosine and formal protonation on one of the carbonyl oxygen atoms of the oxalate moiety of oxaliplatin. This protonation arrangement results in a strong hydrogen bond with the terminal amino nitrogen of carnosine as demonstrated by a 1.315Å bond length, see Figures 7-9. The Pt coordination on the *pros* nitrogen atom of the histidine ring of carnosine is consistent with an earlier study examining the silver ion binding energies of all 20 α-amino

acids, showing that histidine had the third highest silver ion binding energy being lower than that of arginine and only slightly lower than that of lysine.[60] The lowest energy conformer of the Ag^+-histidine complex in that previous study also showed Pt-coordination to the *pros* nitrogen atoms of the histidine ring.[60] Structure **1A**, as shown in Figures 7-9 and Schemes 1-3, is stabilised by three strong hydrogen bonds in addition to the one to the terminal amino nitrogen of the carnosine dipeptides. The number and, more importantly, the strength of these hydrogen bonds, with the longest being 1.886 Å, make structure **1A** to be a relatively rigid conformer. This is evident in the fact that **1A** structure was calculated here to have the lowest entropy value of all conformers of [carnosine + OxPt + H]$^+$ (See Tables S1-S4). This is in line with a previous study that showed structure **1A** to have the second lowest calculated entropy value of twenty five conformers of this complex. [25]

The initial step in the first path proposed for the loss of CO_2 to produce the ion [Carnosine + OxPt – CO_2 + H]$^+$ is shown in Figures 3 and 7 as well as Scheme 1 involves the breaking of the hydrogen bond to the terminal amino nitrogen atom of the carnosine dipeptide and migration of the proton from its initial position on one of the carbonyl oxygen atoms to the other carbonyl atom, both of the oxalate moiety of oxaliplatin (see $\mathbf{TS_{(1A\rightarrow 1B)}}$ in Figure 7 and Scheme 1). These concerted hydrogen bond breaking and hydrogen migration result in the corresponding transition state $\mathbf{TS_{(1A\rightarrow 1B)}}$ to be 48.3 kcal mol^{-1} higher in free energy relative to **1A**. This transition state leads to formation of the minimum structure **1B** (see Figure 7 and Scheme 1), being 8.7 kcal mol^{-1} higher in free energy relative to **1A**, which shows the retention of three of the hydrogen bonds shown in **1A** while no evidence of hydrogen bonding to the terminal amino nitrogen atom is observed. That hydrogen atom is now, in fact, fully migrated to the other carbonyl oxygen atom of the oxalate moiety. A simple rearrangement *via* rotation of the resulting OH group produces the transition state $\mathbf{TS_{(1B\rightarrow 1C)}}$ shown in Figure 7 and Scheme 1 that is calculated to be 20 kcal mol^{-1} higher in energy with

respect to **1A**. This transition state in turn leads to minimum structure **1C** (see Figures 3 and 7 as well as Scheme 1) in which the OH group is rotated. The highest barrier to CO_2 elimination in this mechanism results from the subsequent transition state $\mathbf{TS_{(1C\rightarrow 2A)}}$ (see Figures 3 and 7 as well as Scheme 1), which involves the breakage of the C-C bond of the oxalate moiety and the migration of "inside" proton of the OH group of the oxalate from the oxygen atom to the carbon atom of the newly formed HCOO group. This transition state which involves the simultaneous breaking of two bonds and the formation of a new one is not surprisingly high in energy, presenting a barrier of 71.2 kcal mol^{-1} relative to its associated starting minimum structure **1C**. This transition state leads to the minimum structure **2A**, Figure 7, in which the newly formed HCOO group is attached to the Pt centre through a carbonyl oxygen atom and the CO_2 molecule is now formally eliminated. This released CO_2 molecule is shown in in Figure 7 and Scheme 1 to be held to the amidic hydrogen atom of structure **2A** by a relatively weak hydrogen bond, being the bond length 1.967 Å. Removing the eliminated CO_2 molecule and allowing for simple rotations about single bonds produces conformer **2B** of the ion [Carnosine + OxPt – CO_2 + H]$^+$, which in combination with CO_2 is 8.2 kcal mol^{-1} lower in free energy relative to **2A**. Structure **2B** is shown to be connected to the transition state $\mathbf{TS_{(2B\rightarrow 3A)}}$ in which the Pt-carbonyl oxygen atom bond is broken. This same carbonyl oxygen atom simultaneously abstracts the hydrogen atom of the OH group of carnosine causing the elimination of a HCOOH group and the formation of structure **3A** corresponding to the ion [Carnosine – H + Pt(dach)]$^+$. The highest barrier calculated in this mechanism is for the process of NH_3 elimination from structure **3A** through $\mathbf{TS_{(3A\rightarrow 4A)}}$, which involves two concomitant 1,2-hydrogen shifts and results in the formation of structure **4A** corresponding to the ion [Carnosine – NH_3 – H +Pt(dach)]$^+$ as shown in Figures 3 and 7 as well as Scheme 1. This transition state is shown to be 85.6 kcal mol^{-1} higher in energy than the **1A** global minimum on the PES.

Fragmentation Mechanism 2

The initial step in the second path proposed for the loss of CO_2 from [Carnosine + OxPt + H]$^+$ is shown in Figures 4 and 8 as well as Scheme 2. In analogy with the proposed first mechanism, the initial step here also involves breaking of the hydrogen bond with the terminal amino nitrogen atom of the carnosine dipeptide. However, unlike in mechanism 1, here the proton retained by the carbonyl oxygen atom does not move from its initial position, as shown in structure **TS$_{(1A\rightarrow 1D)}$** in Figure 8 and Scheme 2. This transition state is only 11.1 kcal mol^{-1} higher in free energy relative to the starting structure **1A** and leads, as shown in Figure 8, to formation of structure **1D**, which being internally stabilised by four hydrogen bonds, is higher in free energy relative to structure **1A** by only 3.1 kcal mol^{-1}. Two simple rotations about the H-O and C-C bonds in the oxalate moiety convert structure **1D** into **1E** through the transition state **TS$_{(1D\rightarrow 1E)}$**, whose structure is shown in Figure 8 and Scheme 2, overcoming a free energy barrier of 8.2 kcal mol^{-1} as shown in Figure 4. The elimination of CO_2 from the **1E** conformer of the ion [carnosine + OxPt + H]$^+$ by means of the breakage of the C-C bond of the oxalate moiety and the migration of "inside" proton of the OH group of the oxalate from the oxygen atom to the carbon atom of the newly formed HCOO group takes place via the transition state **TS$_{(1E\rightarrow 2C)}$** in Figure 8 and Scheme 2. This transition state for the elimination of CO_2 involves a free energy barrier of 74.1 kcal mol^{-1} relative to the starting point structure **1E**. This barrier for the elimination of CO_2 is 2.9 kcal mol^{-1} higher in energy than that shown in Figure 3, which details mechanism 1. However, it involves the transition state **TS$_{(1E\rightarrow 2C)}$**, shown in Figure 8 and Scheme 2, which is 6.4 kcal mol^{-1} lower in energy relative to reference energy of the starting structure **1A** on the free energy scale. Like in mechanism 1, here, the transition state **TS$_{(1E\rightarrow 2C)}$** leads to the minimum structure **2C** for the ion [Carnosine + OxPt – CO_2 + H]$^+$ in which the newly formed HCOO group is attached to the Pt centre through a carbonyl oxygen atom and the CO_2 molecule is now formally

eliminated. This eliminated CO_2 molecule is shown in structure **2C** in Figure 8 and Scheme 2 to be held by a very weak hydrogen bond at a distance of 2.289 Å to the hydrogen atom retained by the HCOO group. Removing the eliminated CO_2 molecule and allowing for simple rotations about single bonds produces the same conformer **2B** as in mechanism 1 (see Figure 8 and Scheme 2), which together with CO_2 is 2.1 kcal mol^{-1} lower in free energy relative to **2C**. The remainder of the path of mechanism 2, involving the elimination of HCOOH and NH_3 groups is identical to that described previously in mechanism 1. The formation of structure **4A**, corresponding to the ion [Carnosine – NH_3 – H +Pt(dach)]$^+$ as seen in mechanisms 1 and 2, is shown to involve the highest barriers in these mechanisms. Such barriers, indeed, are 85.6 kcal mol^{-1} higher in free energy relative to the **1A** global minimum on either of these surfaces. This agrees with the energy-resolved CID data which shows the ion [Carnosine – NH_3 – H +Pt(dach)]$^+$ to be produced at significantly high energies and not attaining any significant relative abundance.

Fragmentation Mechanism 3

Both mechanisms 1 and 2 show that the formation of the ion [Carnosine – H + Pt(dach)]$^+$ via the sequential eliminations of CO_2 and HCOOH from [carnosine + OxPt + H]$^+$ entails high free energy barriers of 81.6 and 75.2 kcal mol^{-1}, respectively above the **1A** global minimum. This is, however, not consistent with the energy-resolved CID data shown in Figure 2 which indicates that the ion [Carnosine – H + Pt(dach)]$^+$ is easily produced at low collision energies. This inconsistency led us to investigate a mechanism in which the starting structure **1A** is interconverted to **1D** through the transition state labelled $\mathbf{TS_{(1A\rightarrow 1D)}}$ in the same fashion as in mechanism 2 previously described. Nevertheless, structure **1D** shown in Figure 9 and Scheme 3 in this case undergoes a transformation in which the Pt-O bond connecting the Pt metal to the oxalate moiety is broken and replaced by a Pt bond to the carbonyl oxygen atom of the carnosine dipeptide as shown in structure **1F** in Figure 9 and Scheme 3. This leaves

the oxalate moiety to form a 1.572 Å hydrogen bond through one of its carbonyl oxygen atoms to one of the hydrogen atoms of the amino groups of the dach ligand and another 1.540 Å hydrogen bond through its oxygen atom of its OH group to the hydrogen atom of the OH group the carnosine peptide. This transformation to produce structure **1F** is shown to go through the transition state $\mathbf{TS_{(1D\rightarrow 1F)}}$, which is calculated to be 31.9 kcal mol^{-1} in free energy higher than structure **1A** as shown in Figure 5. Structure **1F** undergoes a simple rotation about a single bond involving a free energy barrier of only 6 kcal mol^{-1} in order to produce structure **1G** in which the OH hydrogen of the oxalate moiety is on the "inside" while both hydrogen bonds to the oxalate moiety are retained. This resulting structure **1G** (see Figure 9 and Scheme 3) is shown to undergo a further transformation by which the "inside" hydrogen atom of oxalate moiety is transferred to the opposing carboxylic oxygen atom of the oxalate while leaving the now formally deprotonated oxygen atom to abstract the hydrogen atom of the OH group of the carnosine peptide. This transformation is shown to take place via the transition state $\mathbf{TS_{(1G\rightarrow 3B)}}$ shown in Figure 9 and Scheme 3 with an associated free energy barrier of only 1.2 kcal mol^{-1} to produce structure **3B** in which the resulting HOC_2O_2OH fragment appears to be attached to the rest of the molecule through a single hydrogen bond formed by one of its hydrogen atoms with a carbonyl oxygen of the carnosine dipeptide. This hydrogen bond is easily broken to eliminate the HOC_2O_2OH group in order to produce the ion $[carnosine + OxPt + H]^+$. The highest free energy barrier to the formation of this ion, by following this fragmentation path, is calculated to be 31.9 kcal mol^{-1} relative to the global minimum structure **1A**, as shown in Figure 5. This is a significantly lower barrier than previously described in mechanisms 1 and 2 for the production of $[Carnosine - H + Pt(dach)]^+$ and is in agreement with the energy-resolved CID data which shows this ion to be easily produced at low collision energies. The subsequent elimination of NH_3 from this ion

to produce the ion [Carnosine – NH_3 – H +Pt(dach)]$^+$ is shown to go through the transition state **TS$_{(3B\rightarrow 4A)}$** which possesses a the relatively high free energy barrier of 99.8 kcal mol^{-1}.

Production of [OxPt + H]$^+$ and [Carnosine + H]$^+$

The energy-resolved CID data shown in Figure 2 clearly indicates that the ion [Carnosine – H + Pt(dach)]$^+$ is the first ion that is produced from the precursor[Carnosine + OxPt + H]$^+$ ion at the lowest dissociation energies. Two other ions are shown to be produced in significant abundances, but at slightly higher dissociation energies. These ions are [OxPt + H]$^+$ and [Carnosine + H]$^+$ which are experimentally generated from the fragmentation of the precursor ion [Carnosine + OxPt + H]$^+$. The pathways to produce [OxPt + H]$^+$ and [Carnosine + H]$^+$ from [Carnosine + OxPt + H]$^+$ were investigated and are shown in Figure 6 where the conformer structure **1A** of the ion [Carnosine + OxPt + H]$^+$ is interconverted into structure 1D through the transition state **TS$_{(1A\rightarrow 1D)}$** previously described in mechanisms 2 and 3. Here, however, structure **1D** is shown to dissociate to produce the combinations Carnosine and [OxPt + H]$^+$ or OxPt and [Carnosine + H]$^+$ via transition states **TS$_{(1D\rightarrow OxPtH)}$** and **TS$_{(1D\rightarrow CarH)}$** calculated to be 42.0 and 52.5 kcal mol^{-1} in free energy higher than structure **1A**, respectively. These relatively low barriers are consistent with the relative ease of production of these two ions experimentally. The relative free energies of the barriers of **TS$_{(1D\rightarrow OxPtH)}$** and **TS$_{(1D\rightarrow CarH)}$** shown in Figure 6 also predicts the production of [OxPt + H]$^+$ to be more favoured at lower energies which is corroborated by the energy-resolved CID data shown in Figure 2.

Conclusions

In this paper, collision-induced dissociation experiments on the protonated carnosine-oxaliplatin complex, [Carnosine + OxPt + H]$^+$ using several collision energies were shown to yield nine different fragment ions. Generation of the product [Carnosine – H + Pt(dach)]$^+$ ion

from [Carnosine + OxPt + H]$^+$ is shown to be the lowest energy process. This agrees well with our calculations as shown in mechanism 3 where the generation of [Carnosine – H + Pt(dach)]$^+$ ion via the direct loss of HOC_2O_2OH from [Carnosine + OxPt + H]$^+$ involves the smallest energy barrier calculated here being 31.9 kcal mol^{-1}. Two other pathways were calculated for the generation of [Carnosine – H + Pt(dach)]$^+$ through the sequential losses of CO_2 and HCOOH from [Carnosine + OxPt + H]$^+$ and were shown to involve significantly higher barriers being 81.6 and 75.2 kcal mol^{-1} respectively as shown in mechanisms 1 and 2. At slightly higher collision energies the loss of neutral carnosine from [Carnosine + OxPt + H]$^+$ to produce [OxPt + H]$^+$ was experimentally observed, followed by the loss of oxaliplatin from the same precursor ion to produce [Carnosine + H]$^+$. This corresponds well with the two calculated pathways for the generation of these observed ions were the barriers for the production of [OxPt + H]$^+$ and [Carnosine + H]$^+$ were shown to be 42.0 and 52.5 kcal mol^{-1}, respectively. At significantly higher energies, the ion [OxPt – CO_2 + H]$^+$ was shown to be initially formed, while the last two investigated ions [Carnosine + OxPt – CO_2 + H]$^+$ and [Carnosine – NH_3 – H +Pt(dach)]$^+$ were shown not attain any significant relative abundance. The calculated barriers for the generation of these two latter ion was shown to be 75.2 and 85.6 kcal mol^{-1} respectively.

Acknowledgements

The authors would like to thank the American University in Cairo for the funding sponsorship and provision of resources for the Project. The Dipartimento di Chimica e Tecnologie Chimiche of Università della Calabria is gratefully acknowledged.

References

[1] W. Gulewitsch, S. Amiradzibi, *Ber. Deut. Chem. Ges.* **1900**, *33*, 1902-1903.

[2] I. Severina, O. Bussygina, N. Pyatakova, *Biochemistry-Moscow* **2000**, *65*, 783-788.

[3] R. Kohen, Y. Yamamoto, K. Cundy, B. Ames, *Proc. Natl. Acad. Sci. U. S. A.* **1988**, *85*, 3175-3179.

[4] S. E. Gariballa, A. J. Sinclair, *Age and Aging* **2000***, 29***,** 207-210.

[5] M. Horning, L. Blakemore, P. Trombley, *Brain Res.* **2000**, *852*, 56-61.

[6] M. Nino, *Journal of cosmetics, dermatological sciences and applications* **2011***, 1*, 177.

[7] L. J. Hobart, I. Seibel, G. S. Yeargans, N. W. Seidler, *Life Sci.* **2004**, *75*, 1379-1389.

[8] A. R. Hipkiss, J. E. Preston, D. T. Himsworth, V. C. Worthington, M. Keown, J. Michaelis, J. Lawrence, A. Mateen, L. Allende, P. A. Eagles, N. J. Abbott, *Ann NY Acad. Sci.* **1998**, *854*, 37- 53.

[9] G. A. McFarland, R. Holliday, *Exp. Gerontol.* **1999**, *34*, 35-45.

[10] V. P. Reddy, M. R. Garrett, G. Perry, M. A. Smith, *Sci. Aging Knowledge Environ.* **2005**, *18*, pe12.

[11] J. Kovacs-nolan, Y. Mine, In Animal Muscle-Based Bioactive Peptides; Bioactive Proteins and Peptides as Functional Foods and Nutraceuticals; Wiley-Blackwell: **2010**; pp 225-231.

[12] Y. Suzuki, O. Ito, N. Mukai, H. Takahashi, K. Takamatsu, *Jpn. J. Physiol.* **2002**, *52*, 199-205.

[13] A. Boldyrev, S. Severin, *Advances in enzyme regulation* **1990**, *30*, 175.

[14] M. Babizhayev, *Biochim. Biophys. Acta* **1989**, *1004*, 363-371.

[15] J. Kang, K. Kim, S. Choi, H. Kwon, M. Won, T. Kang, *Mol. Cells* **2002**, *13*, 498-502.

[16] C. Corona, V. Frazzini, E. Silvestri, R. Lattanzio, R. La Sorda, M. Piantelli, L. M. T. Canzoniero, D. Ciavardelli, E. Rizzarelli, S. L. Sensi, *PLoS ONE* **2011**, *6*, e17971.

[17] K. Seto, T. Yoneta, H. Suda, H. Tamaki, *Biochem. Pharmacol.* **1999**, *58*, 245-250.

[18] S. Kato, A. Tanaka, Y. Ogawa, K. Kanatsu, K. Seto, T. Yoneda, K. Takeuchi, *Med. Sci. Monit.* **2001**, *7*, 20-25.

[19] A. Mahmood, A. J. FitzGerald, T. Marchbank, E. Ntatsaki, D. Murray, S. Ghosh, R. J. Playford, *Gut* **2007**, *56*, 168-175.

[20] S. Stvolinsky, M. Kukley, D. Dobrota, M. Vachova, I. Tkac, A. Boldyrev, *Cell. Mol. Neurobiol.* **1999**, *19*, 45-56.

[21] A. Boldyrev, S. L. Stvolinsky, O. V. Tyulina, V. B. Koshelev, N. Hori, D. O. Carpenter, *Cellular and Molecular Neurobiology* **1997***, 17*, 259-271.

[22] A. Renner, N. Zemitzsch, B. Fuchs, K. D. Geiger, M. Hermes, J. Hengstler, R. Gebhardt, J. Meixensberger, F. Gaunitz, *Mol. Cancer* **2010**, *9*, 2.

[23] A. Iovine, M. L. Iannella, F. Nocella, M. R. Pricolo, M. A. Bevilacqua, *Cancer Lett.* **2012**, *315*, 122-128.

[24] Y. Horii, J. Shen, Y. Fujisaki, K. Yoshida, K. Nagai, *Neurosci. Lett.* **2012**, *510*, 1-5.

[25] E. M. Moustafa, C. L. Camp, A. S. Youssef, A. Amleh, H. J. Reid, B. L. Sharp, T. Shoeib, *Metallomics* **2013**, *5*, 1537-1546.

[26] C. G. Hartinger, M. Groessl, S. M. Meier, A. Casini, P. J. Dyson, *Chem. Soc. Rev.* **2013**, *42*, 6186.

[27] M. Groessl, C. G. Hartinger, *Anal. Bioanal. Chem.*, **2013**, *405*, 1791.

[28] S. L. Kerr, T. Shoeib, B. L. Sharp, *Anal. Bioanal. Chem.*, **2008**, *391*, 2339.

[29] T. Shoeib**,** S.E. Taylor, G.D. Jones, A. L. Thomas, J. P. Wood, H. J. Reid, B. L. Sharp, *Int. J. Mass Spec.* **2011**, *307*, 70.

[30] A. Zayed, G. D. Jones, H. J. Reid, T. Shoeib, S. E. Taylor, A. L. Thomas, J. P. Wood, B. L. Sharp, *Metallomics*, **2011**, *3*, 991.

[31] H. Li, J. R. Snelling, M. P. Barrow, J. H. Scrivens, P. J. Sadler, P. B. O'Connor, *J. Am. Soc. Mass Spec.*, **2014**, *25*, 1217.

[32] T. Zhao, F. L. King, *J. Am. Soc. Mass Spec.*, **2009**, *20*, 1141.

[33] K. Ossipov, Y. Y. Scaffidi-Dominallo, I. F. Seregina, M. Galanski, B. K. Keppler, A. R. Timerbaev, M. A. Bolshov, *J. Inorg. Biochem.*, **2014**, *137*, 40-45.

[34] A. R. Timerbaev, S. S. Aleksenko, K. Polec-Pawlak, R. Ruzik, O. Semenova, C. G. Hartinger, S. Oszwaldoski, M. Galanski, M. Jarosz, B. K. Keppler, *Electrophoresis*, **2004**, *25*, 1988.

[35] C. Brauckmann, C. A. Wehe, M. Kieshauer, C. Lanvers-Kaminsky, M. Sperling, U. Karst, *Anal. Bioanal. Chem.*, **2013**, *405*, 1855-1864.

[36] R. Miao, G. Yang, Y. Miao, Y. Mei, J. Hong, C. Zhao, L. Zhu, *Rapid. Commun. Mass Spectrom.*, **2005**, *19*, 1031-1040.

[37] A. D. Becke, *J. Chem. Phys.* **1993**, *98*, 5648–5652.

[38] A. Lee, W. Yang, R. G. Parr, *Phys. Rev. B* **1988**, *37*, 785-789.

[39] D. Becke, *Phys. Rev. A* **1988**, *38*, 3098-3100.

[40] Stephens, P. J.; Devlin, F. J.; Chabalowski, C. F.; Frisch, M. J. *J. Phys. Chem.* **1994**, *98*, 11623–11627.

[41] M. J. Frisch, G. W. Trucks, H. B. Schlegel, G. E. Scuseria, M. A. Robb, J. R. Cheeseman, G. Scalmani, V. Barone, B. Mennucci, G. A. Petersson, H. Nakatsuji, M. Caricato, X. Li, H. P. Hratchian, A. F. Izmaylov, J. Bloino, G. Zheng, J. L. Sonnenberg, M. Hada, M. Ehara, K. Toyota, R. Fukuda, J. Hasegawa, M. Ishida, T. Nakajima, Y. Honda, O. Kitao, H. Nakai, T. Vreven, J. A. Montgomery Jr, J. E. Peralta, F. Ogliaro, M. Bearpark, J. J. Heyd, E. Brothers, K. N. Kudin, V. N. Staroverov, R. Kobayashi, J. Normand, K. Raghavachari, A. Rendell, J. C. Burant, S. S. Iyengar, J. Tomasi, M. Cossi, N. Rega, J. M. Millam, M. Klene, J. E. Knox, J. B. Cross, V. Bakken, C. Adamo, J. Jaramillo, R. Gomperts, R. E. Stratmann, O. Yazyev, A. J. Austin, R. Cammi, C. Pomelli, J. W. Ochterski, R. L. Martin, K. Morokuma, V. G. Zakrzewski, G. A. Voth, P. Salvador, J. J. Dannenberg, S. Dapprich, A. D. Daniels,O¨ . Farkas, J.B. Foresman, J. V. Ortiz, J.Cioslowski and D. J. Fox, Gaussian 09, Revision A.1, Gaussian, Inc., Wallingford CT, 2009.

[42] P. J. Hay, W. R. Wadt, *J. Chem. Phys.* **1985**, *82*, 270-283.

[43] W. R. Wadt, P. J. Hay, *J. Chem. Phys.* **1985**, *82*, 284-298.

[44] P. J. Hay, W. R. Wadt, *J. Chem. Phys.* **1985**, *82*, 299-310.

[45] T. Shoeib, D. W. Atkinson, B. L. Sharp, *Inorg. Chim. Acta* **2010**, *363*, 184-192.

[46] M. Belcastro, T. Marino, N. Russo, M. Toscano, *J. Inorg. Biochem.* **2009**, *103*, 50-57.

[47] L. Salassa, H. I. A. Phillips, P. J. Sadler, *Phys. Chem. Chem. Phys.* **2009**, *11*, 10311-10316.

[48] R. Wysokinski, J. Kuduk-Jaworska, D. Michalska, *J. Mol. Struct.: Theochem* **2006**, *758*, 169-179.

[49] A. B. Yongye, M. A. Giulianotti, A. Nefzi, R. A. Houghten, K. Martinez-Mayorga, *J. Comput. Aided Mol. Des.* **2010**, *24*, 225-235.

[50] N.T. Abdel-Ghani, A.M. Mansour, *Eur. J. Med. Chem.* **2012**, *47*, 399-411.

[51] R. Wysokinski, D. Michalska, *J. Comput. Chem.* **2001**, *22*, 901-912.

[52] Giese, G. Deacon, J. Jaworska, D. McNaughton, *Biopolymers* **2002**, *67*, 294-297.

[53] T. C. Shore, D. Mith, D. DePrekel, S. McNall, Y. Ge, *Reac. Kinet. Mech. Cat.* **2013**, *109*, 315-333.

[54] A. Vacher , F. Barrière , F. Camerel , J. F. Bergamini , T. Roisnel , D. Lorcy , *Dalton Trans.* **2013**, *42*, 383-394.

[55] A. I. Oprea, F. Moscalu, A. Dumbrava, S. Ioannou, A. Nicolaides, M.A. Girtu, *Romanian Journal of Physics* 2011, 56, 125-133.

[56] R. J. Holmes, R. A. J. O'Hair, W. D. McFadyen, *Rapid Commun. Mass Spectrom.* **2000**, *14*, 2385-2392.

[57] G-Y Lee, M-S Jun, *Bull. Korean Chem. Soc.* **2001**, *22*, 11-12.

[58] Y. Kaya, C.Icsel, V.T. Yilmaz, O. Buyukgungor, *Journal of Organometallic Chemistry* **2014**, *752*, 83-90.

[59] L. Pazderski, J. Tousek, J. Sitkowski, K. Malinakova, L. Kozerski, E. Szlyk, *Magn. Reson. Chem.* **2009**, *47*, 228-238.

[60] N. Moldovan, P. Lönnecke, I. Silaghi-Dumitrescu, L. Silaghi-Dumitrescu, E. Hey-Hawkins, *Inorg. Chem.* **2008**, *47*, 1524-1531.

[61] A. Kerényi, V. Kovács, T. Körtvélyesi, K. Ludányi, L. Drahos, G. Keglevich, *Heteroatom Chem.* **2010**, *21*, 63-70.

[62] Y.-W. Huang, S.-L. Lee, *Chem. Phys. Lett.* **2010**, *492*, 98-102.

[63] T. Shoeib, B. L. Sharp, *Inorg. Chim. Acta.* **2013**, *405*, 258-264.

[64] J. A. R. Navarro, M. A. Romero, J. M. Salas, M. Quiros, J. El Bahraoui, J. Molina, *Inorg. Chem.* **1996**, *35*, 7829-7835.

[65] R. Pazout, J. Houskova, M. Dusek, J. Maixner, P. Kacer, *Struct. Chem.* **2011**, *22*, 1325-1330.

[66] R. Rajeev, R. B. Sunoj, *Dalton Trans.* **2012**, *41*, 8430-8440.

[67] T. Shoeib, B. L. Sharp, *Metallomics* **2012**, *4*, 1308-1320.

[68] E. M. Moustafa, M. Korany, N. A. Mohamed, T. Shoeib, *Inorganica Chimica Acta* **2014**, *421*, 123-135.

[69] J. Roithová, D. Schröder, *Chem. Rev.* **2010**, *110*, 1170-1211.

[70] Fukui, K. *J. Phys. Chem.* **1970**, *74*, 4161–4163.

[71] Gonzalez, C.; Schlegel, H. B. *J. Chem. Phys.* **1989**, *90*, 2154–2161.

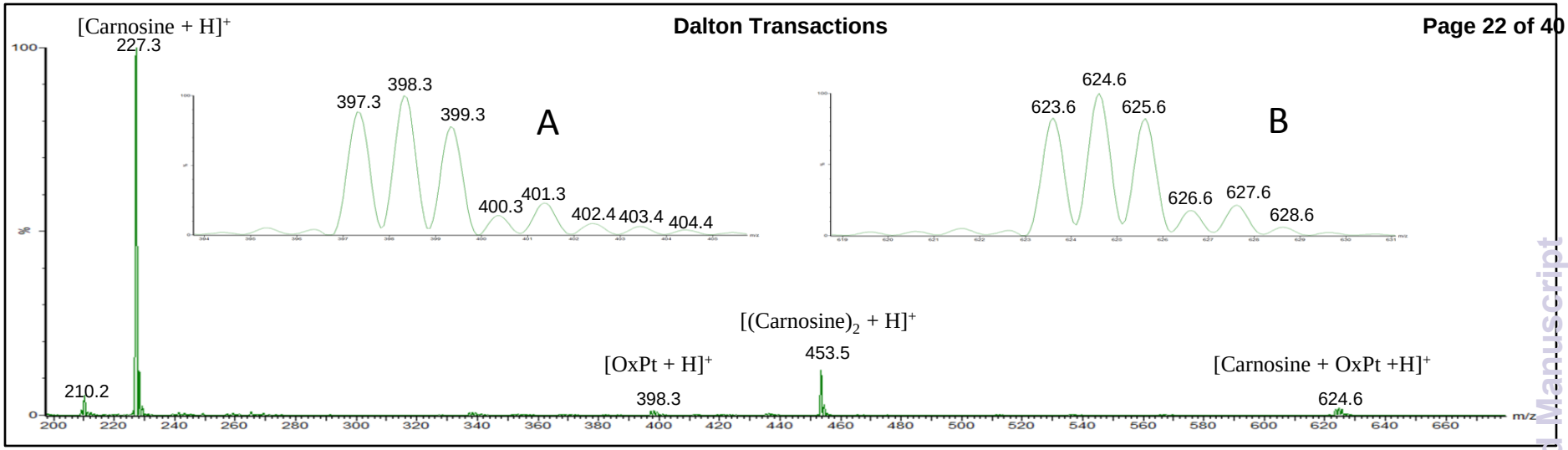

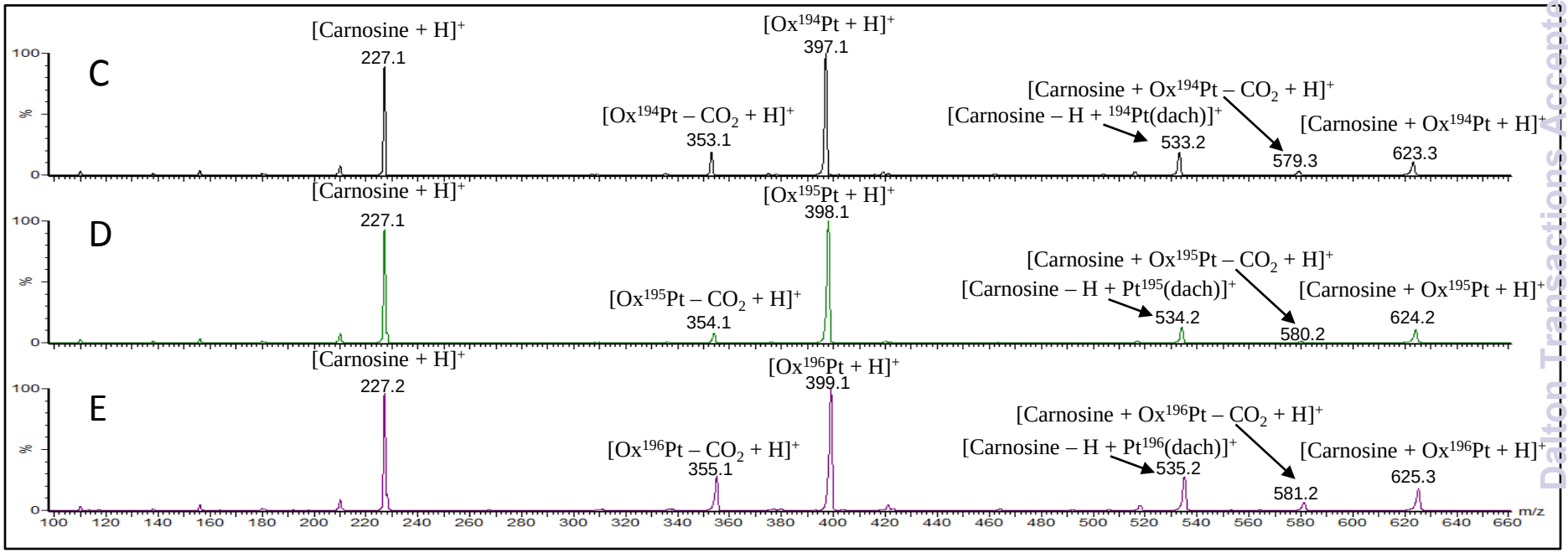

Figure 1: Top Panel, full scan MS spectrum of a (2:1) molar mixture of Carnosine and OxPt in a (1:1) (v/v) water/methanol solution as without allowing for incubation time. The signals assigned as $[OxPt + H]^+$ and $[Carnosine + OxPt + H]^+$ are each expanded and normalized to 100% in inserts A and B respectively for clarity. Bottom Panel, MS^2 spectrum of the ion $[Carnosine + OxPt + H]^+$ generated at 25 eV in the lab frame. Panels C, D and E show the CID patterns obtained due to the isotopes ^{194}Pt, ^{195}Pt and ^{196}Pt of $[Carnosine + OxPt + H]^+$ respectively.

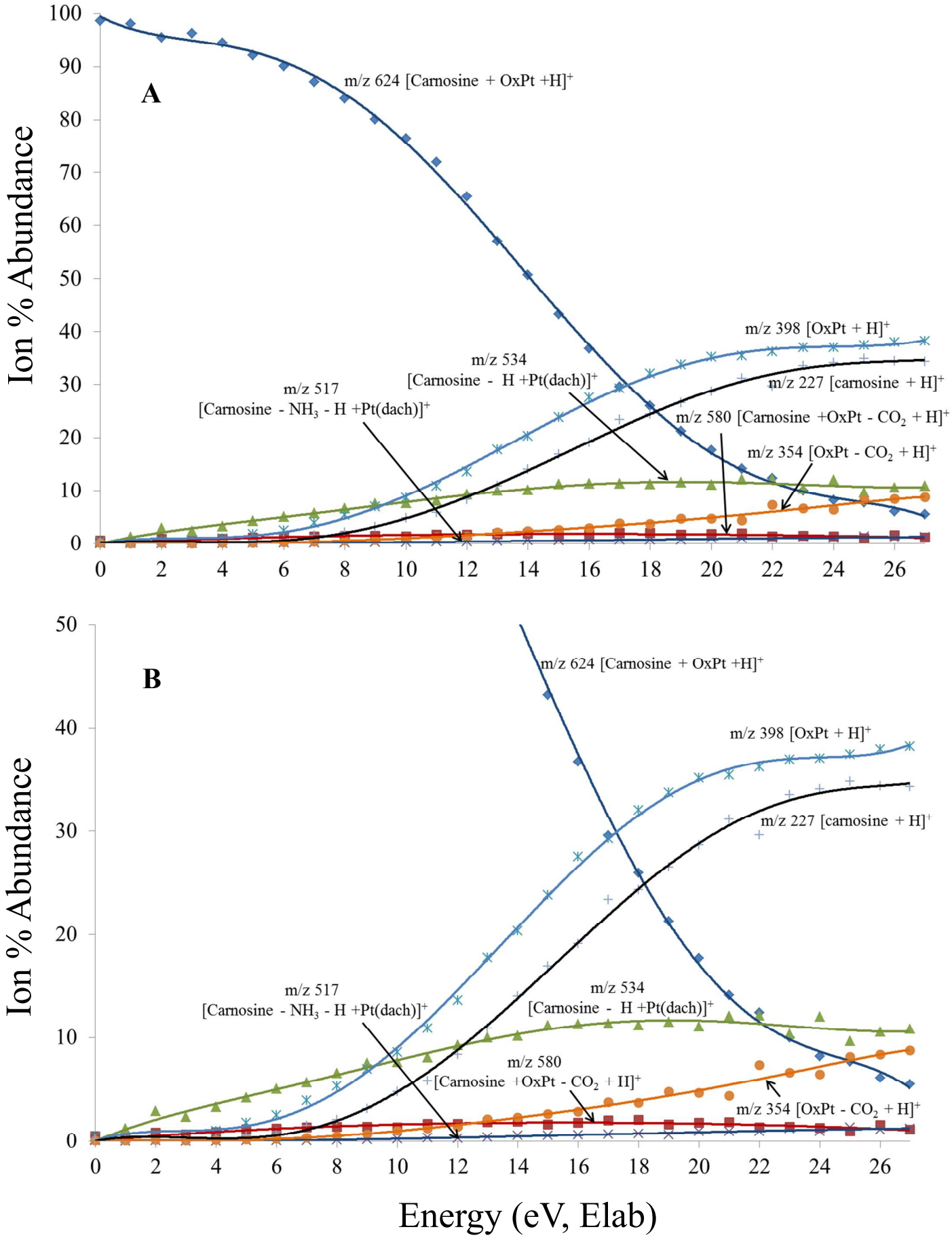

Figure 2: Energy-resolved collision induced dissociation curves of [Carnosine + OxPt +H]$^+$. Y-axis are (ion abundance)/(total ion abundance) expressed as a percentage, m/z values refer to complexes containing ^{195}Pt. Panel A shows the full curve while panel B shows an expanded view for clarity.

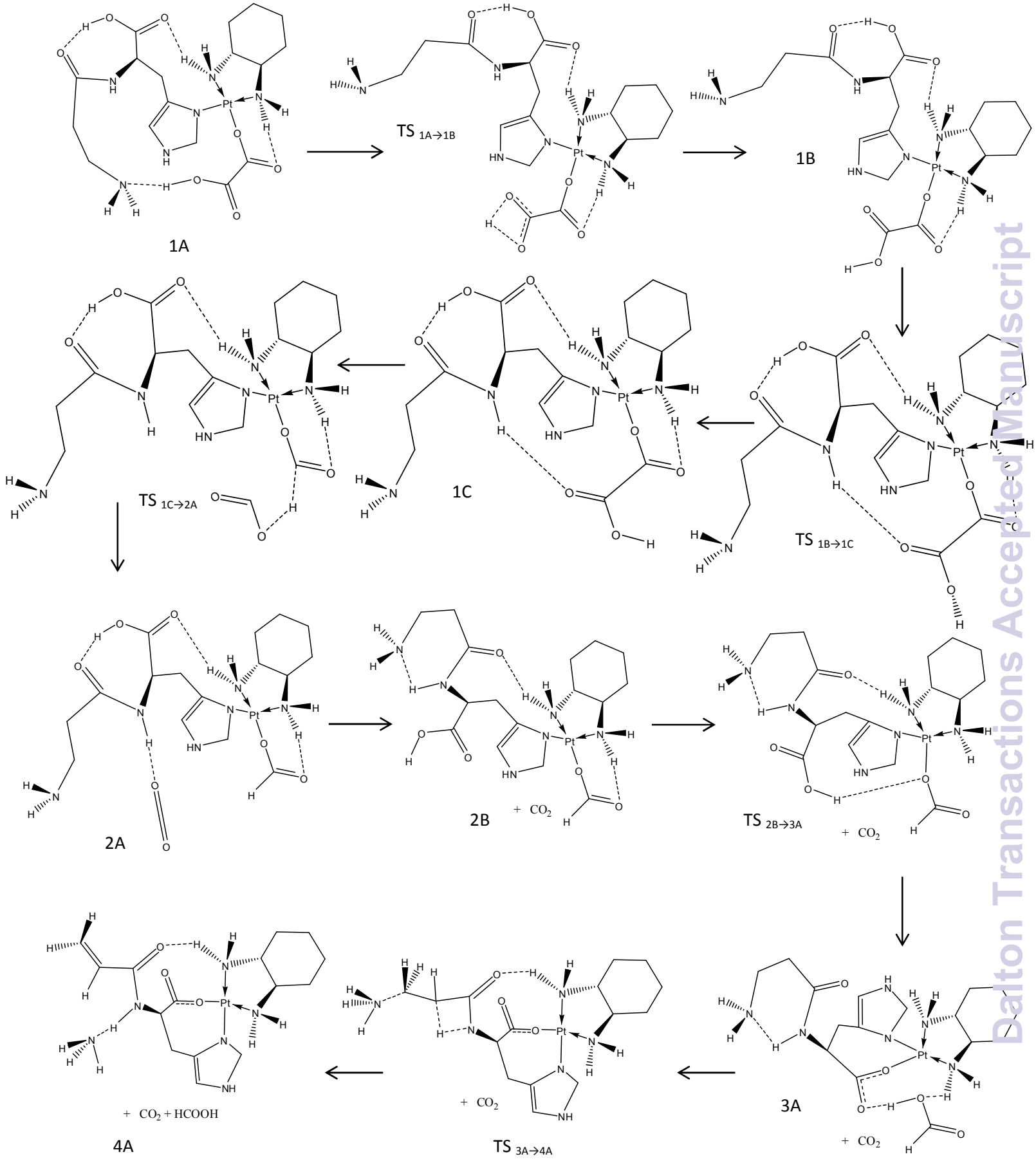

Scheme 1: Proposed mechanism 1 for the collision induced fragmentation of [Carnosine + Oxaliplatin + H]$^+$.

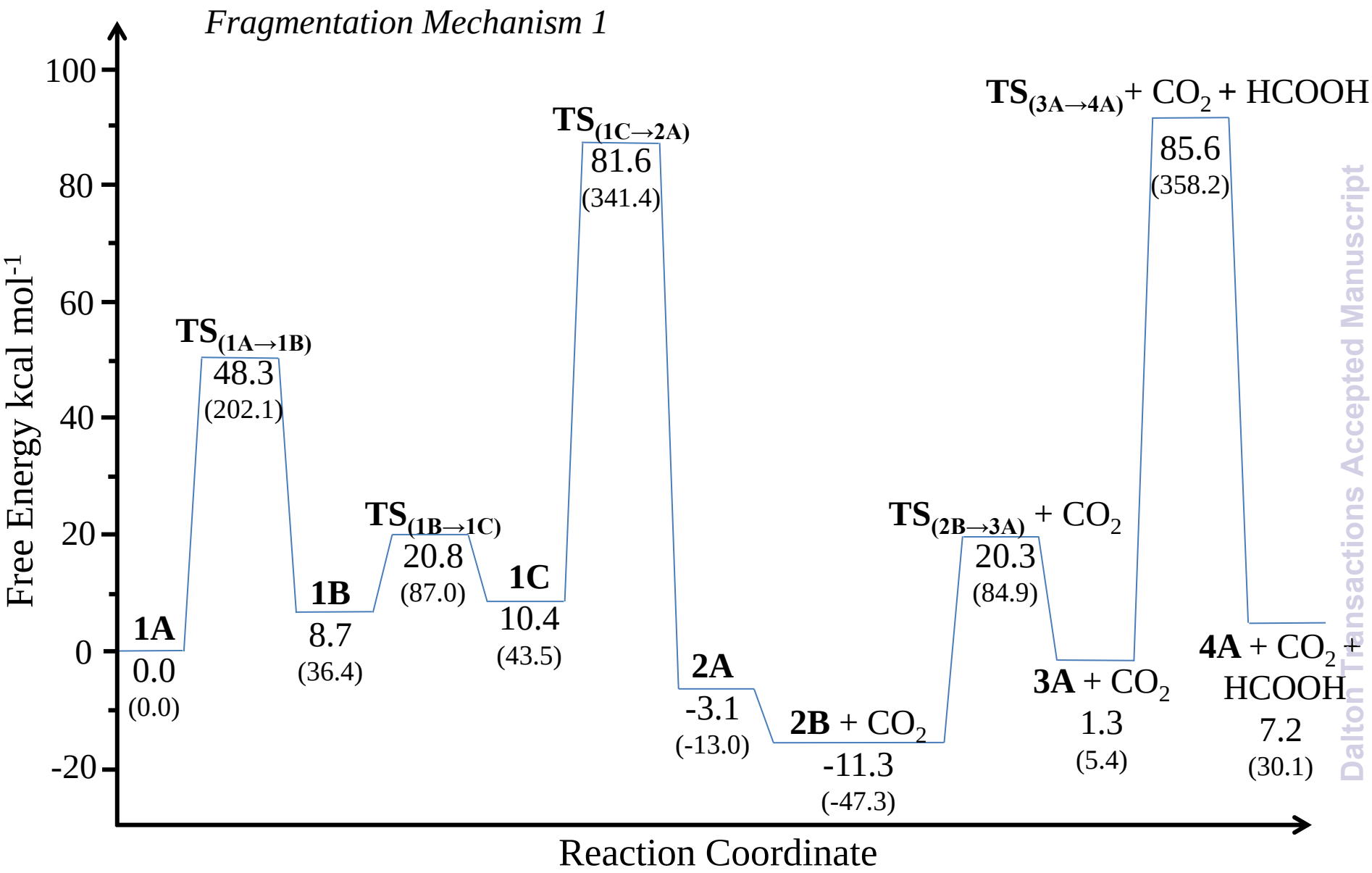

Figure 3: Potential energy surface for the fragmentation of the protonated carnosine-oxaliplatin complex, ion 1A. Structure labels are in bold, top numbers are in kcal mol^{-1} while bottom numbers in parentheses are in kJ mol^{-1}.

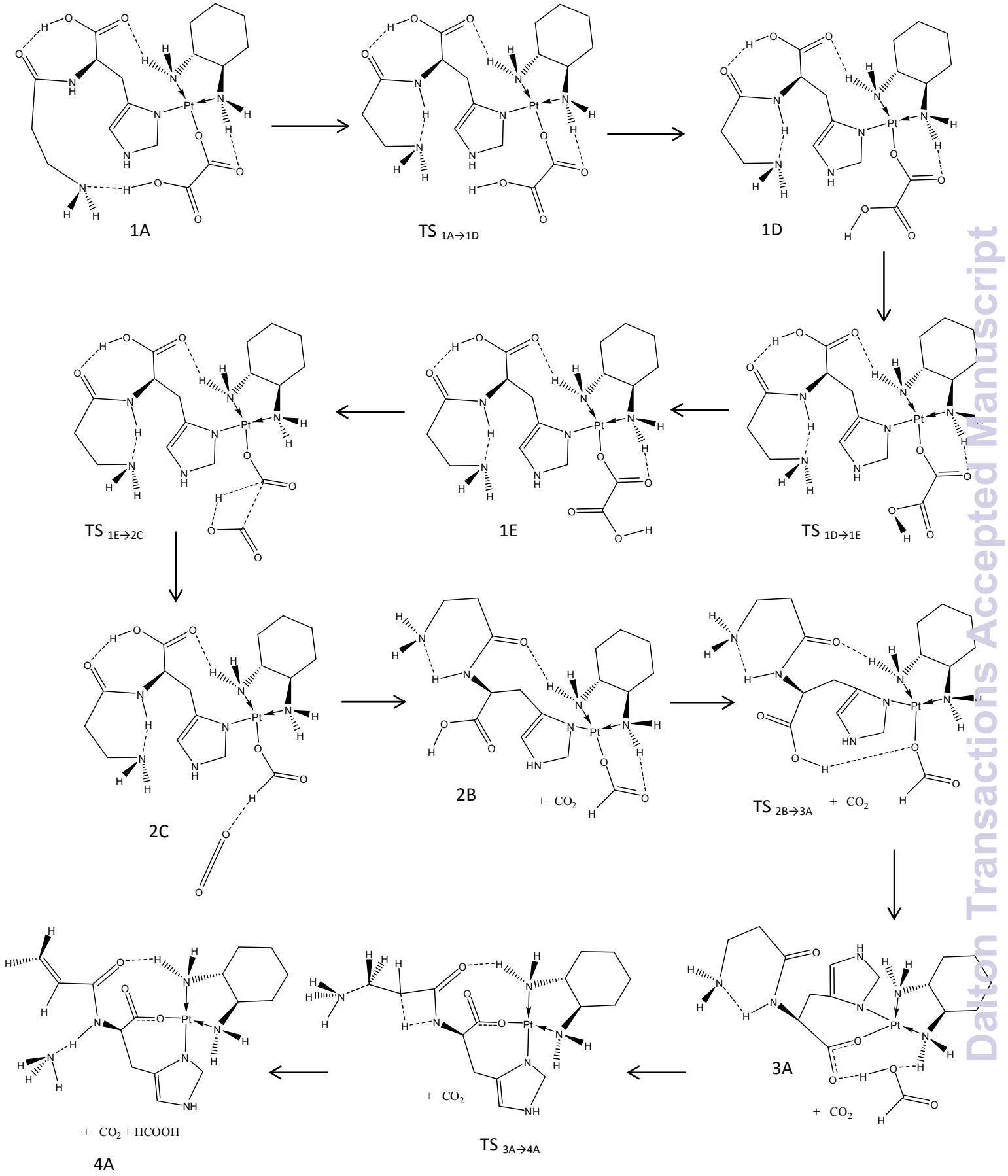

Scheme 2: Proposed mechanism 2 for the collision induced fragmentation of [Carnosine + Oxaliplatin + H]$^+$.

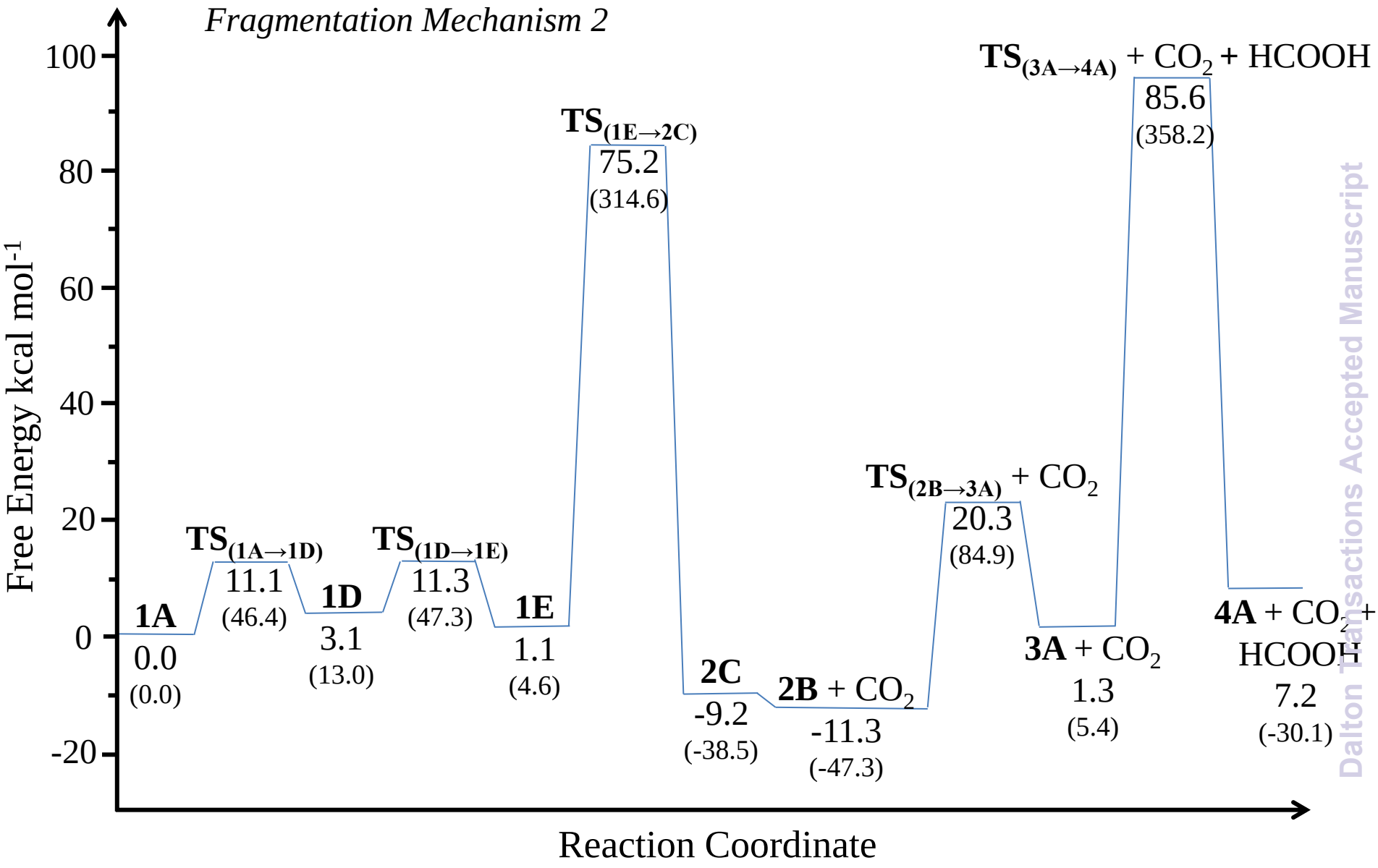

Figure 4: Potential energy surface for the fragmentation of the protonated carnosine-oxaliplatin complex, ion 1A. Structure labels are in bold, top numbers are in kcal mol^{-1} while bottom numbers in parentheses are in kJ mol^{-1}.

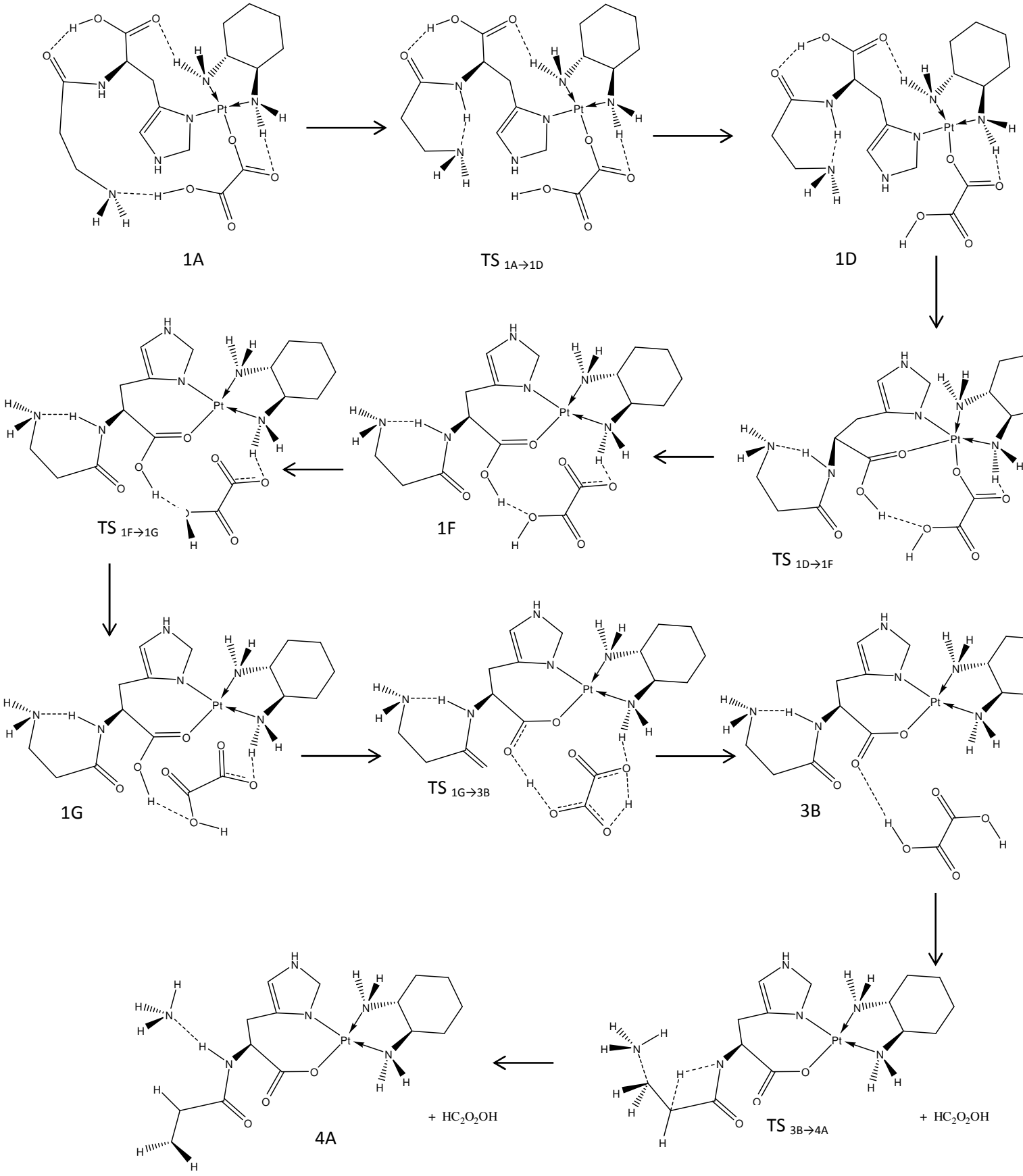

Scheme 3: Proposed mechanism 3 for the collision induced fragmentation of [Carnosine + Oxaliplatin + H]$^+$.

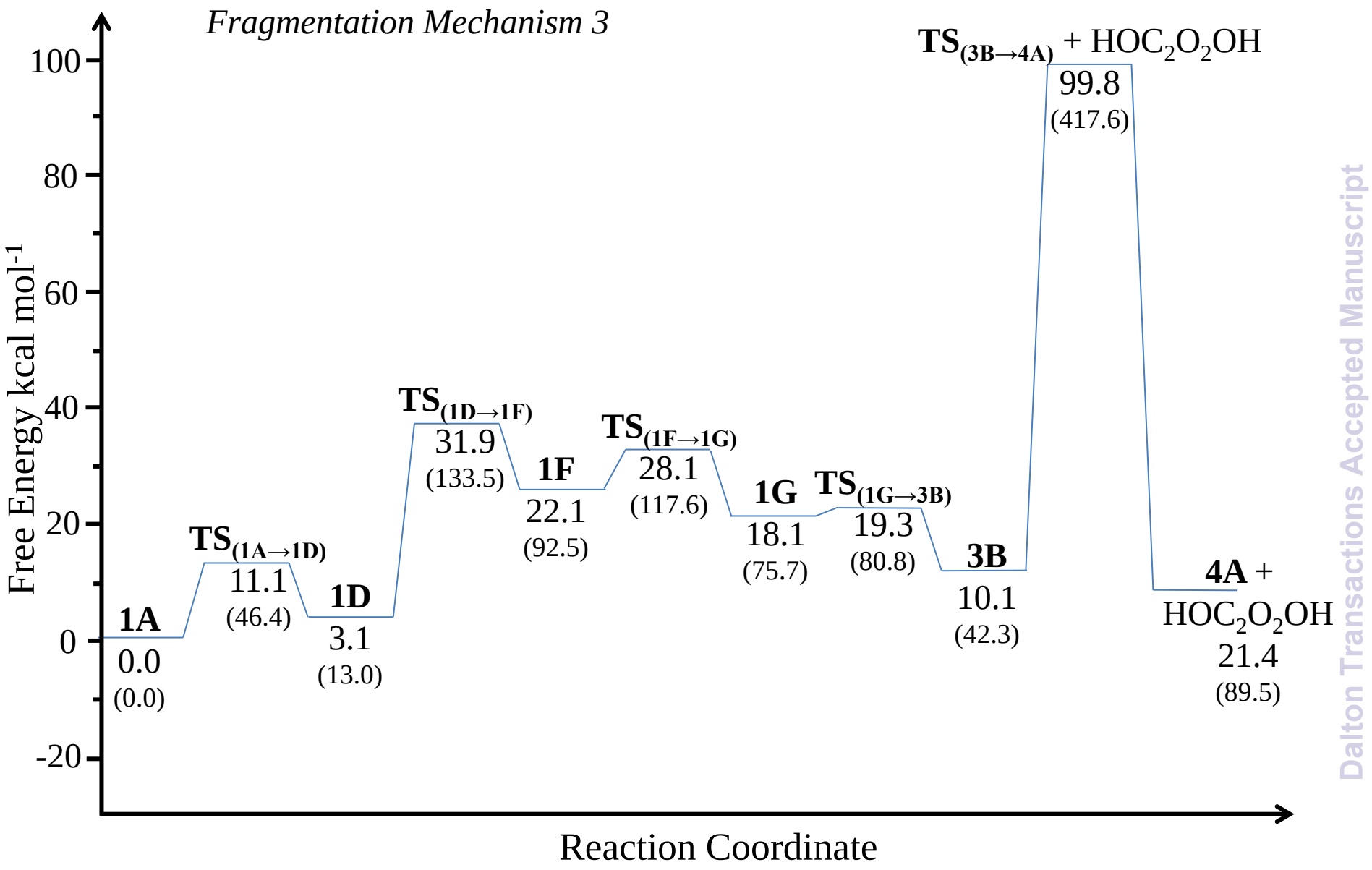

Figure 5: Potential energy surface for the fragmentation of the protonated carnosine-oxaliplatin complex, ion 1A. Structure labels are in bold, top numbers are in kcal mol^{-1} while bottom numbers in parentheses are in kJ mol^{-1}.

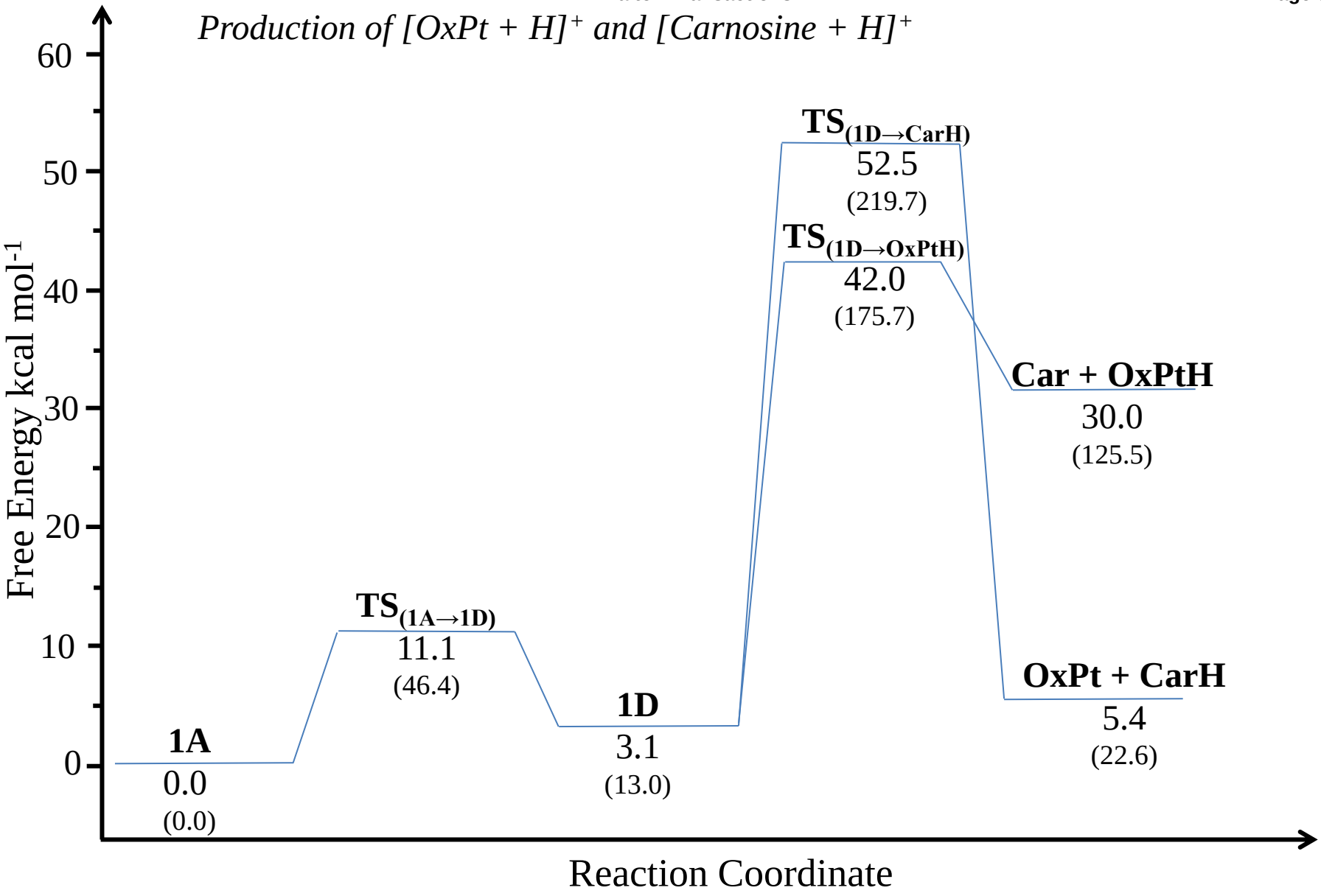

Figure 6: Potential energy surface for the fragmentation of the protonated carnosine-oxaliplatin complex, ion 1A. Structure labels are in bold, top numbers are in kcal mol^{-1} while bottom numbers in parentheses are in kJ mol^{-1}.

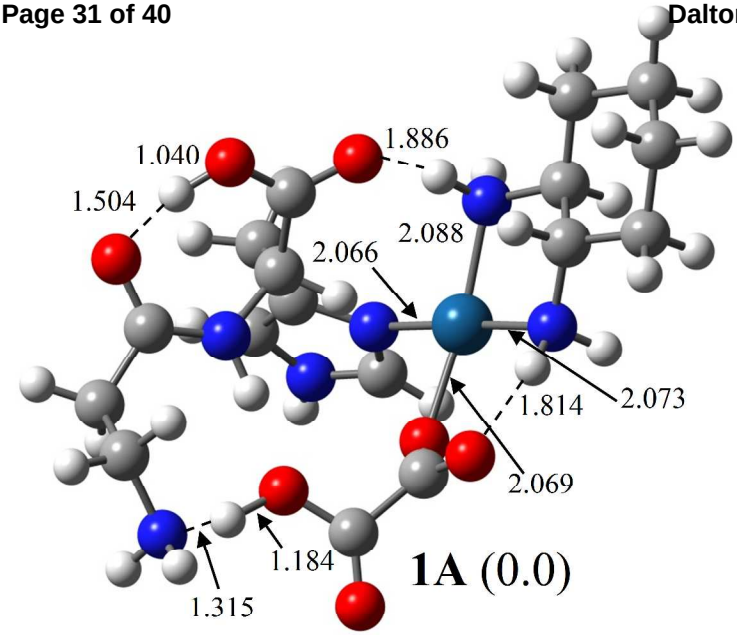

1A (0.0)

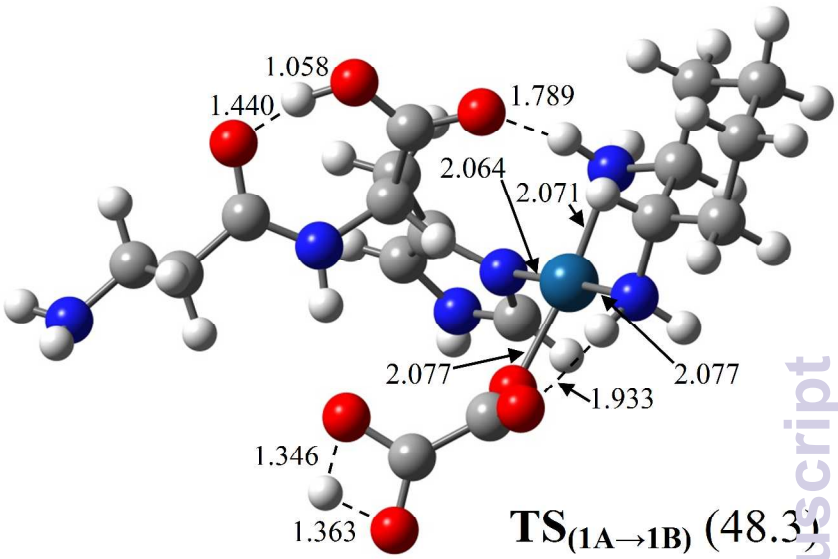

TS$_{(1A→1B)}$ (48.3)

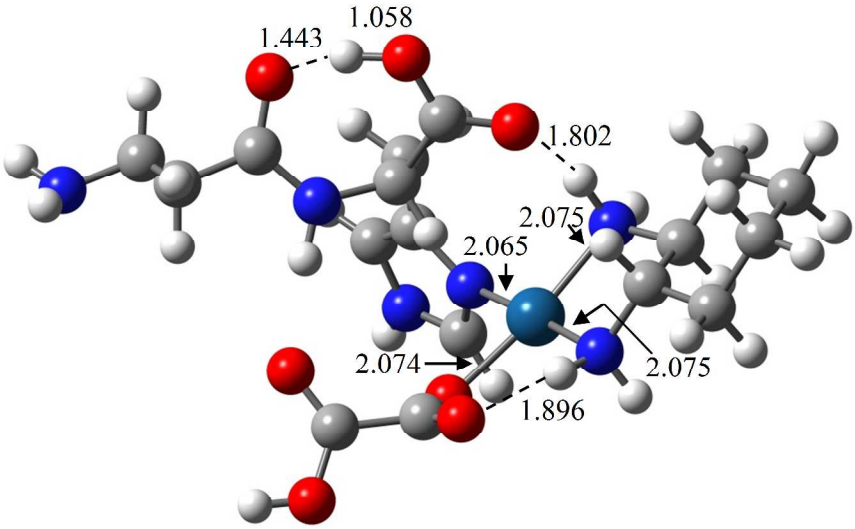

1B (8.7)

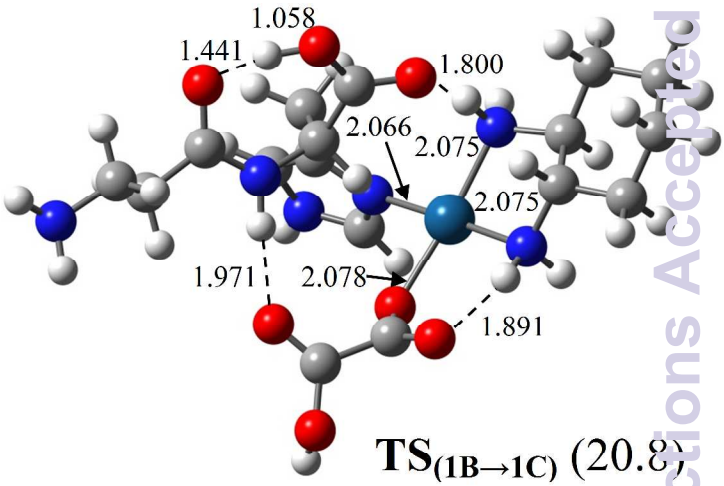

TS$_{(1B→1C)}$ (20.8)

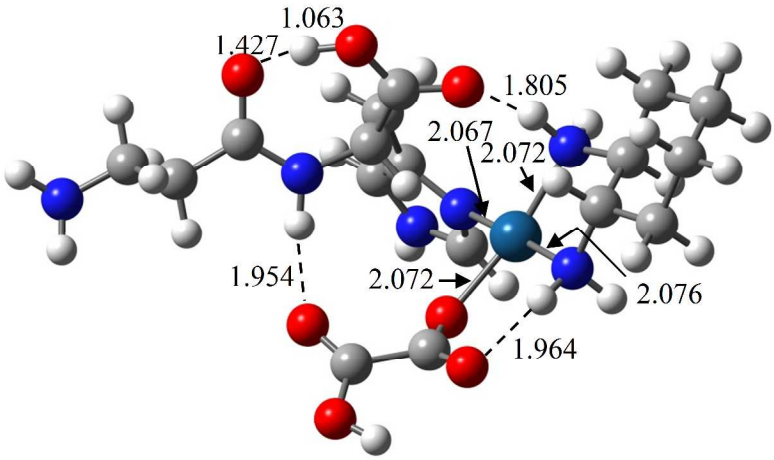

1C (10.4)

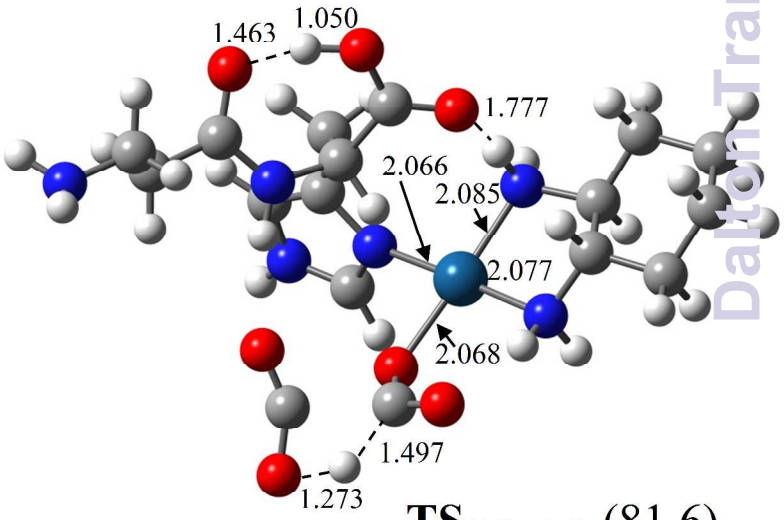

TS$_{(1C→2A)}$ (81.6)

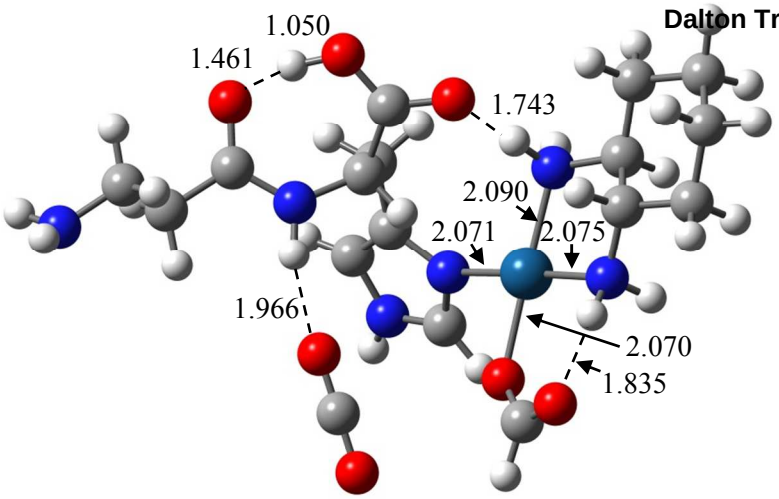

2A (-3.1)

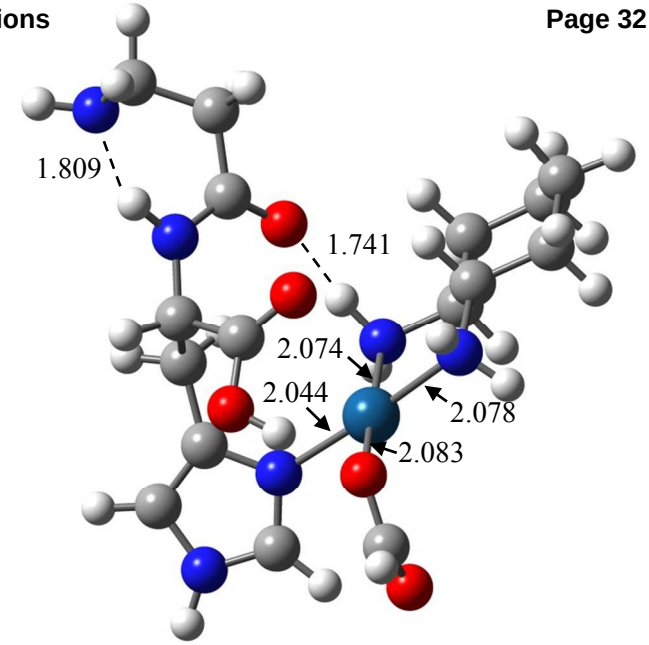

2B + CO_2 (-11.3)

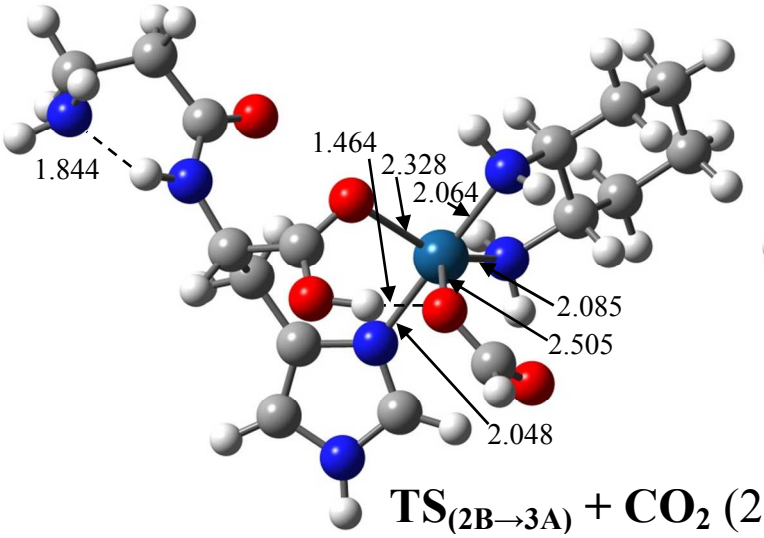

$TS_{(2B→3A)}$ + CO_2 (20.3)

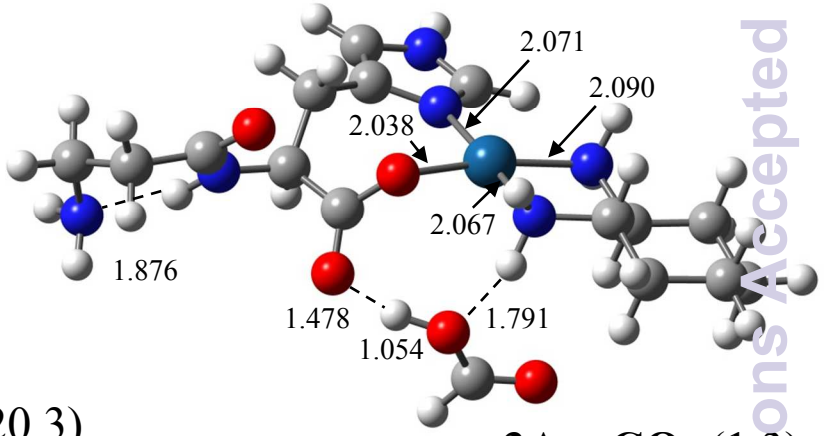

3A + CO_2 (1.3)

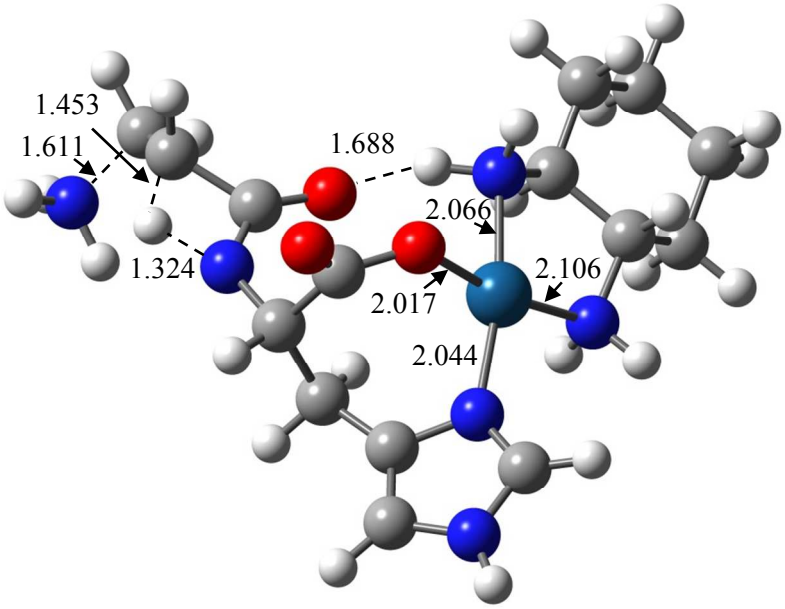

$TS_{(3A→4A)}$ + CO_2 + HCOOH (85.6)

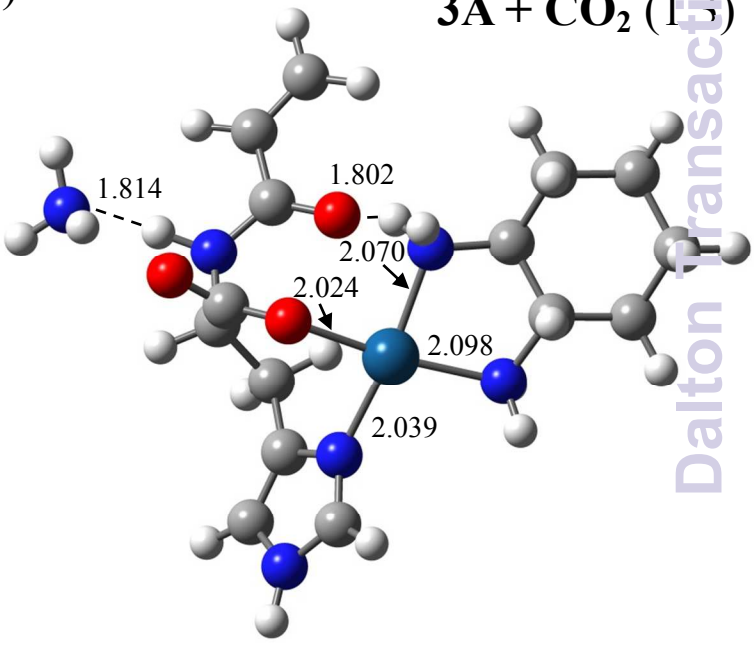

4A + CO_2 + HCOOH (7.2)

Figure 7: Structures corresponding to the fragmentation mechanism described in Figure 4. All structures are calculated at the B3LYP/LANL2DZ level of theory. Bond lengths are in Angstroms, relative free energies are indicated in parenthesis. Gray, red, blue and white spheres represent carbon, oxygen, nitrogen and hydrogen atoms respectively.

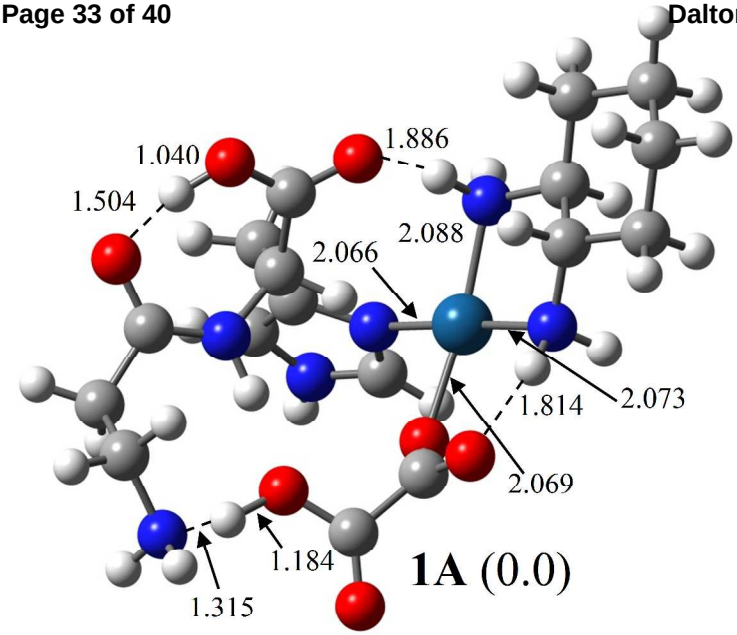

1A (0.0)

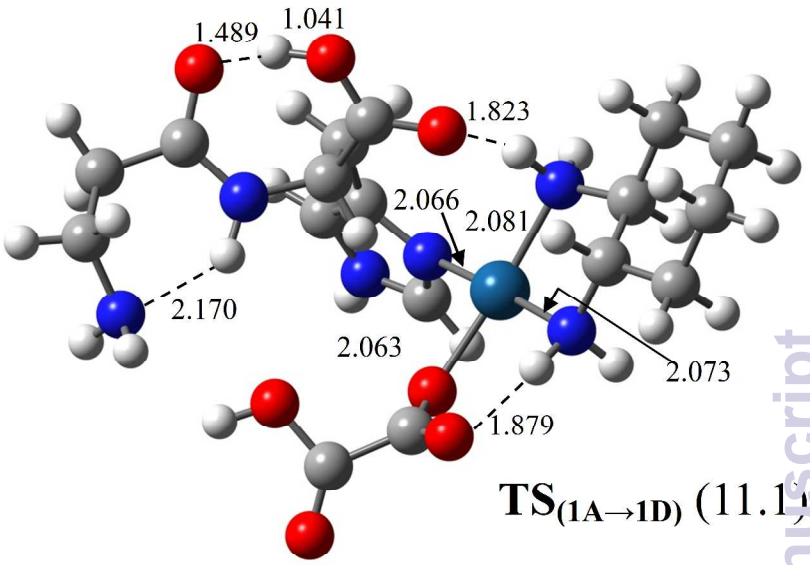

TS$_{(1A\rightarrow 1D)}$ (11.1)

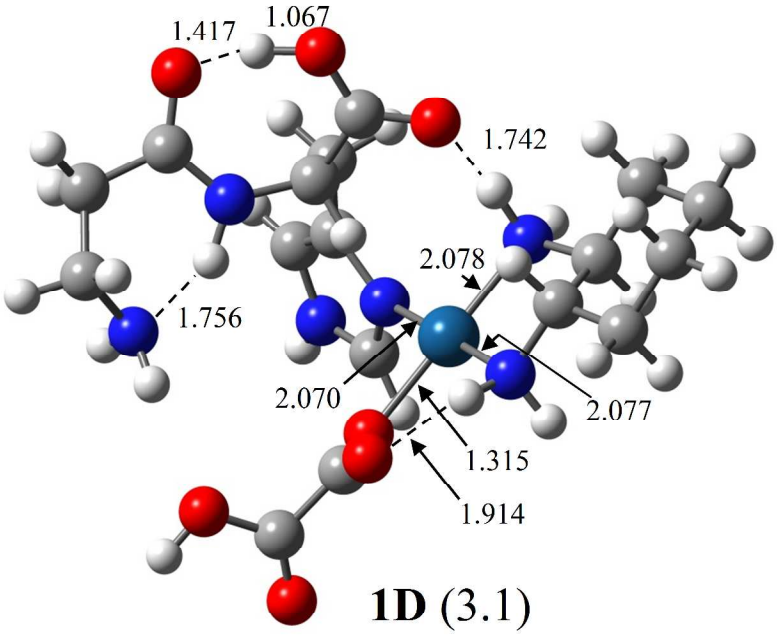

1D (3.1)

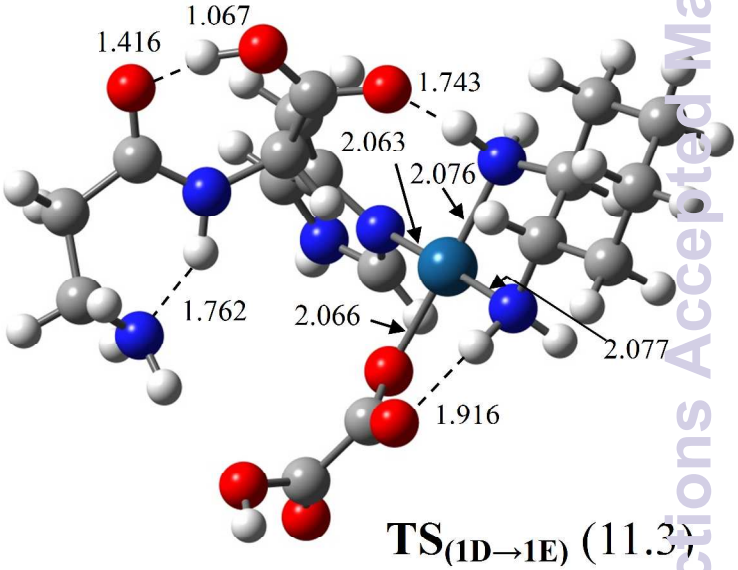

TS$_{(1D\rightarrow 1E)}$ (11.3)

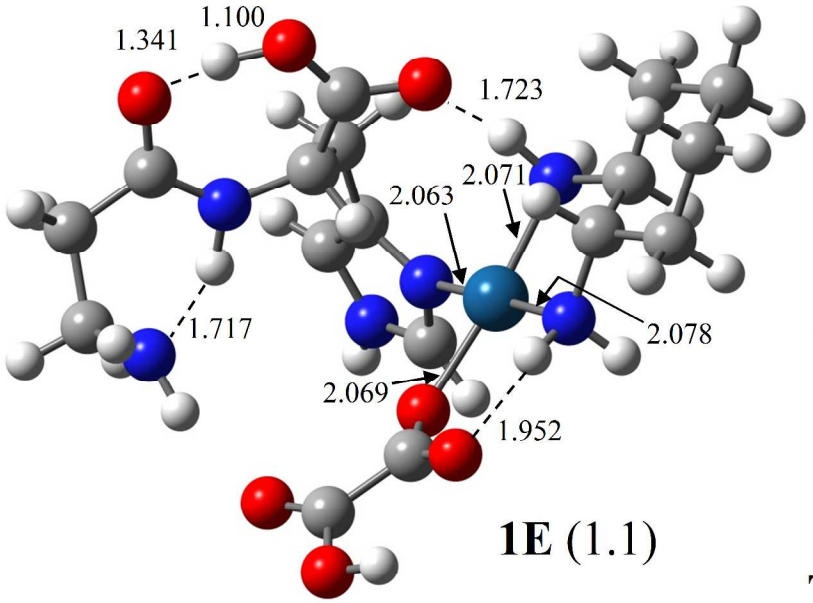

1E (1.1)

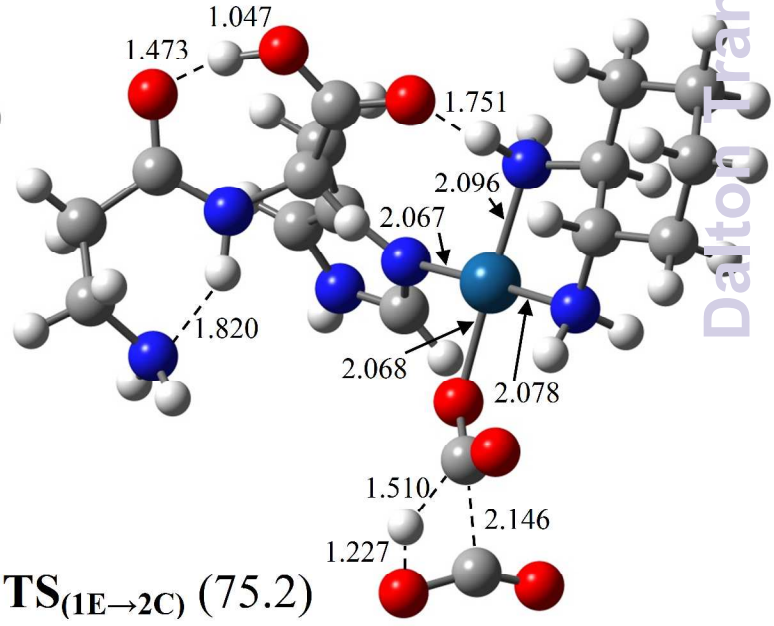

TS$_{(1E\rightarrow 2C)}$ (75.2)

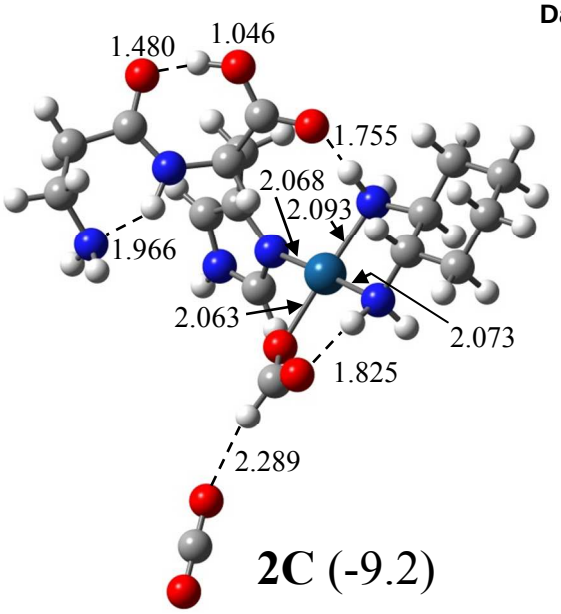

2C (-9.2)

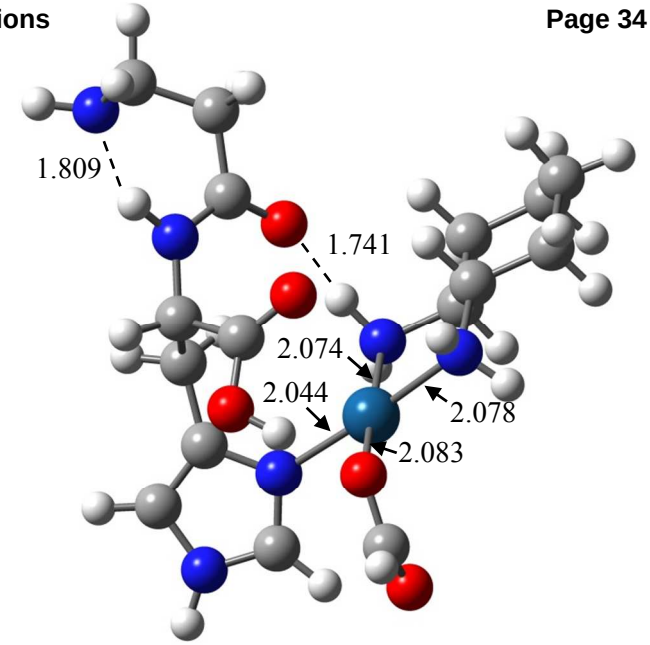

2B + CO_2 (-11.3)

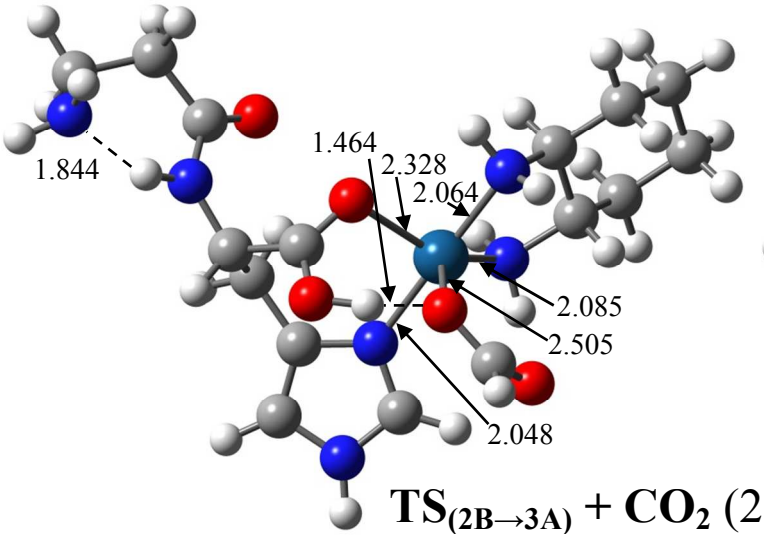

$TS_{(2B→3A)}$ + CO_2 (20.3)

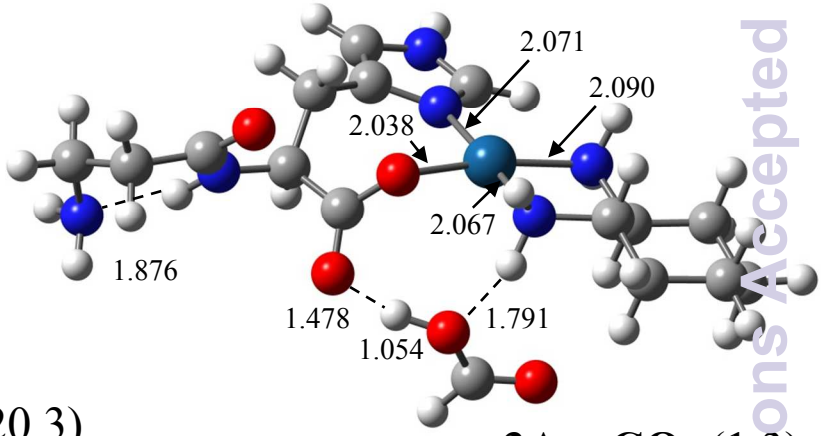

3A + CO_2 (1.3)

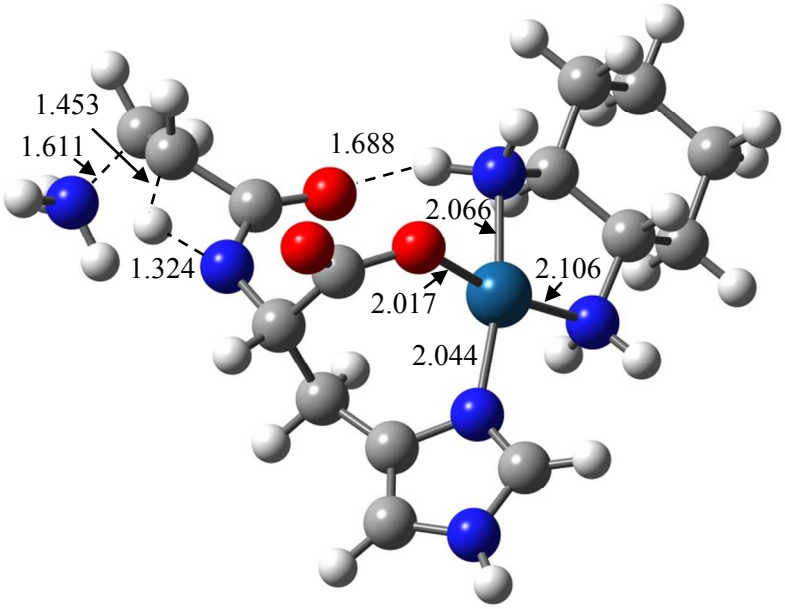

$TS_{(3A→4A)}$ + CO_2 + HCOOH (85.6)

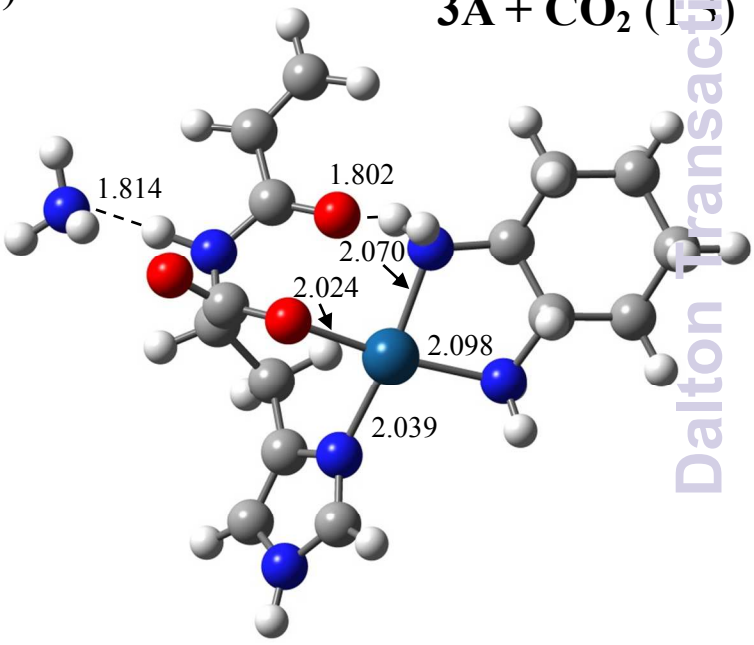

4A + CO_2 + HCOOH (7.2)

Figure 8: Structures corresponding to the fragmentation mechanism described in Figure 5. All structures are calculated at the B3LYP/LANL2DZ level of theory. Bond lengths are in Angstroms, relative free energies are indicated in parenthesis. Gray, red, blue and white spheres represent carbon, oxygen, nitrogen and hydrogen atoms respectively.

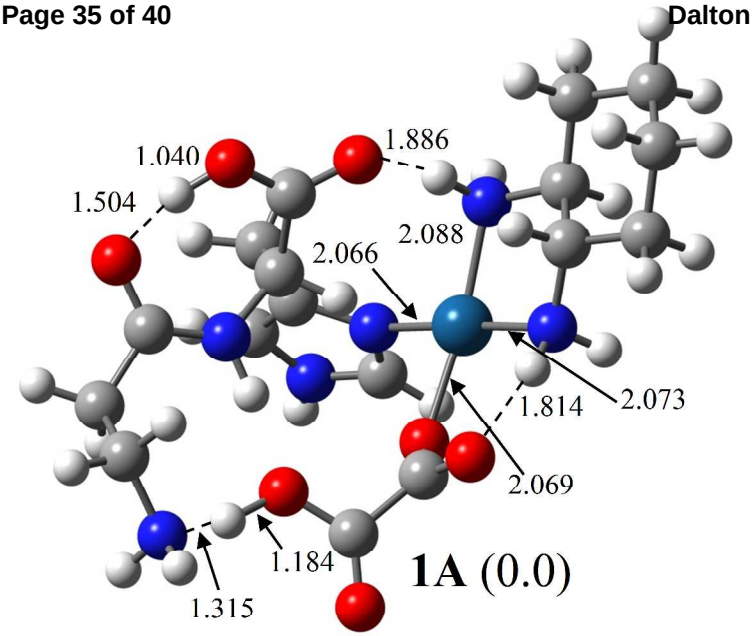

1A (0.0)

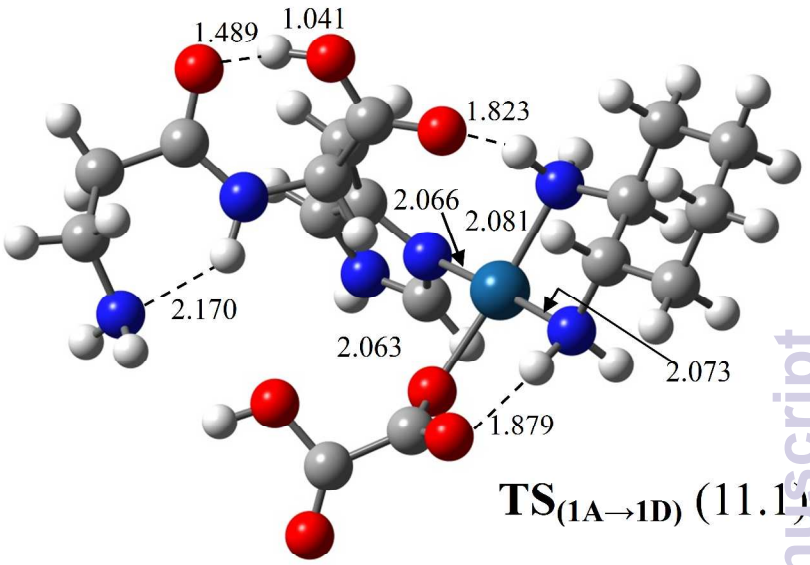

TS$_{(1A→1D)}$ (11.1)

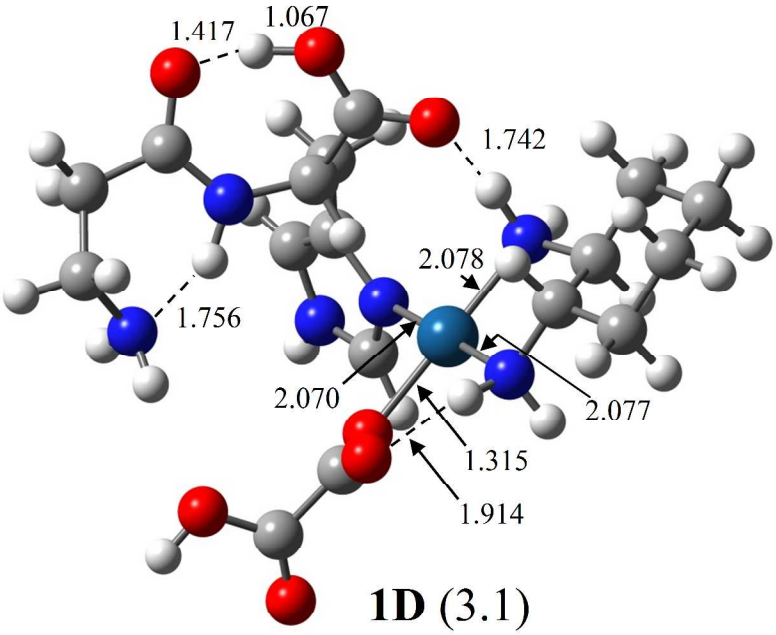

1D (3.1)

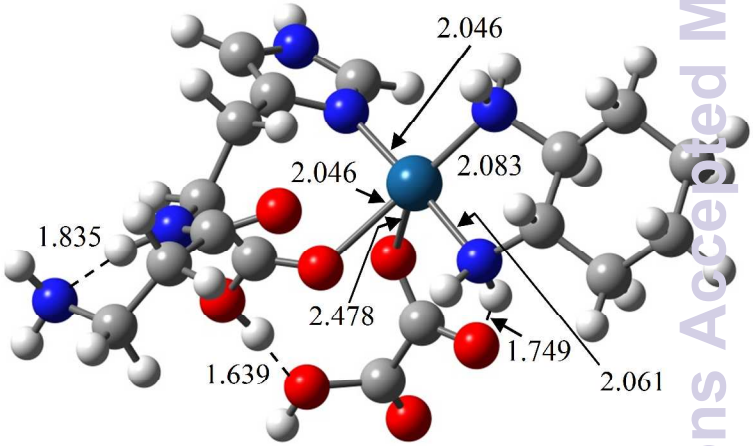

TS$_{(1D→1F)}$ (31.9)

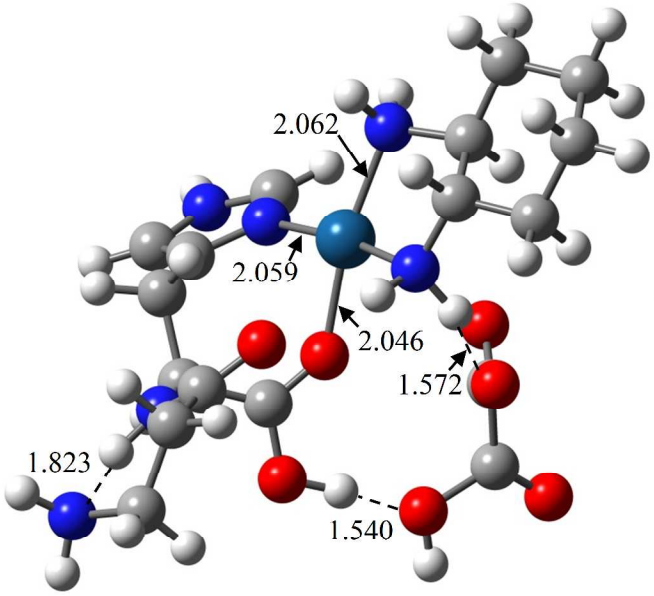

1F (22.1)

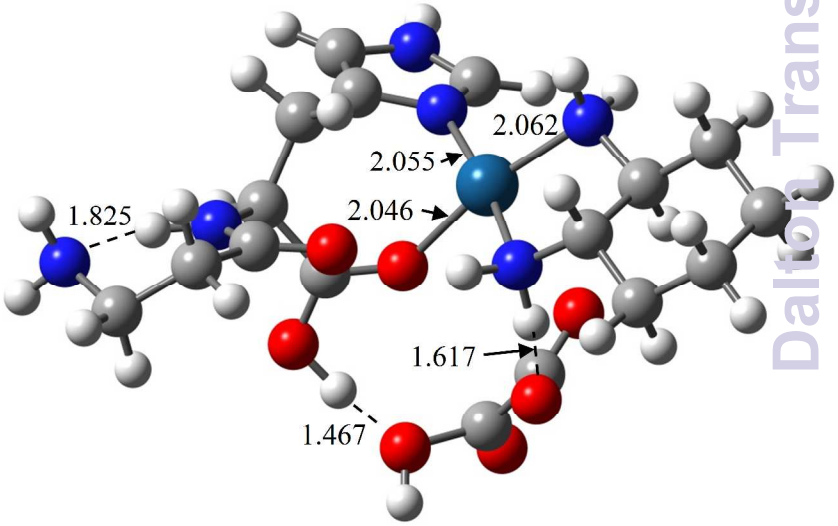

TS$_{(1F→1G)}$ (28.1)

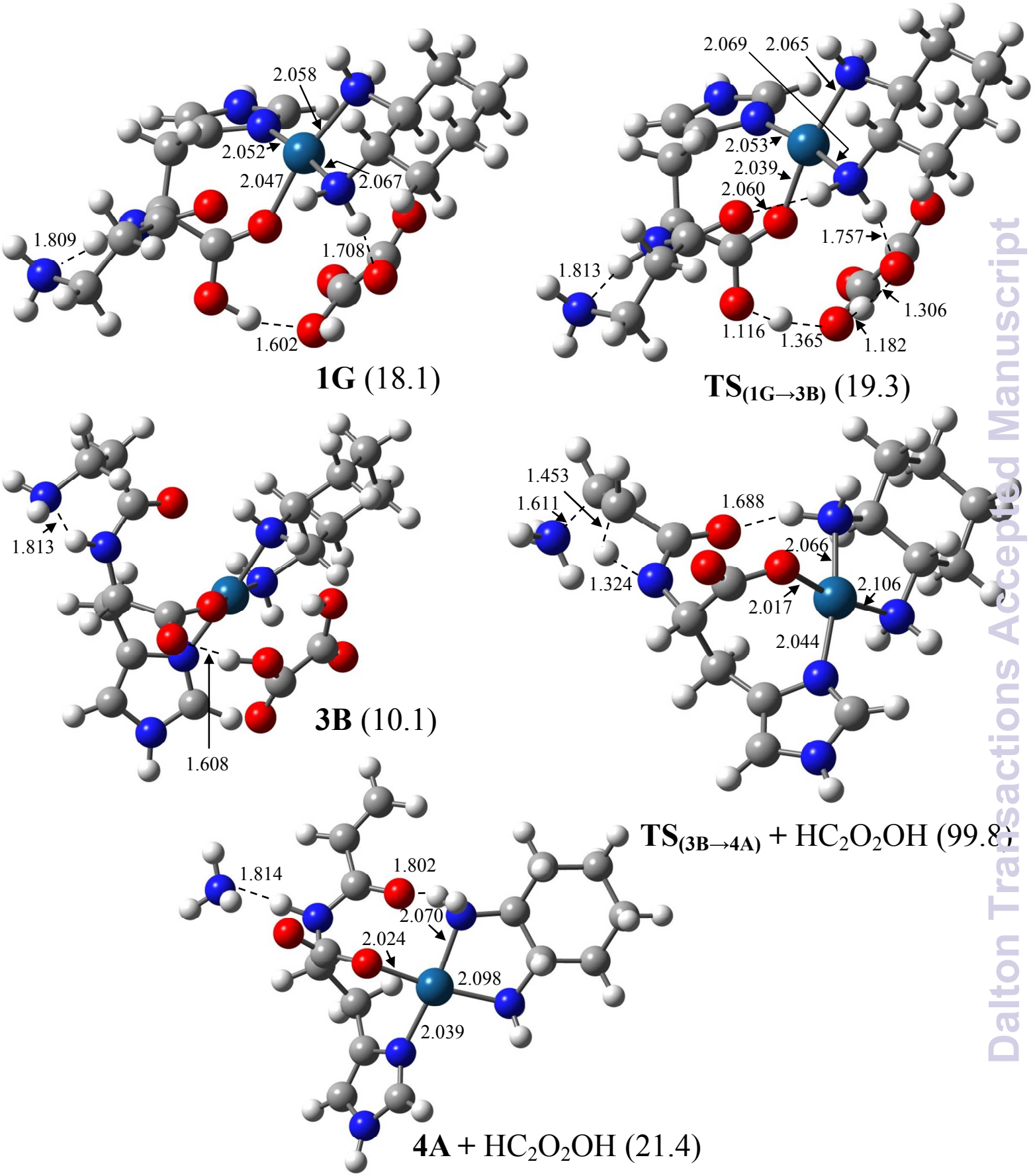

Figure 9: Structures corresponding to the fragmentation mechanism described in Figure 6. All structures are calculated at the B3LYP/LANL2DZ level of theory. Bond lengths are in Angstroms, relative free energies are indicated in parenthesis. Gray, red, blue and white spheres represent carbon, oxygen, nitrogen and hydrogen atoms respectively.

Table S1: Electronic energies, Zero-Point Vibrational Energies, Thermal Energies, Entropies and relative free energies for species calculated at B3LYP\LANL2DZ for structures described in Figures 3 and 7. Italicized relative free energy values are in kcal mol^{-1} while values in parentheses are in kJ mol^{-1}.

Structure	Electronic energy (Hartrees)	ZPE (kcal mol^{-1})	$\mathbf{H^o_{298} - H^o_0}$ (kcal mol^{-1})	Entropy (cal mol^{-1} K^{-1})	Relative free energy at 298 K
1A	-1639.2886242	312.6	19.6	196.8	*0.0* (0.0)
$TS_{(1A\rightarrow1B)}$	-1639.2026501	309.3	20.5	207.5	*48.3* (202.1)
1B	-1639.2708451	312.4	20.5	207.6	*8.7* (36.4)
$TS_{(1B\rightarrow1C)}$	-1639.2497207	311.1	20.5	206.8	*20.8* (87.0)
1C	-1639.2682279	312.3	20.5	206.6	*10.4* (43.5)
$TS_{(1C\rightarrow2A)}$	-1639.1456481	307.1	20.9	210.0	*81.6* (341.4)
2A	-1639.2843606	311.4	21.4	218.1	*-3.1* (-13.0)
2B + CO_2	-1639.288777	312.0	20.5	235.1	*-11.3* (-47.3)
$TS_{(2B\rightarrow3A)}$ + CO_2	-1639.232367	309.8	20.6	241.0	*20.3* (84.9)
3A + CO_2	-1639.262436	310.4	20.9	244.4	*1.3* (5.4)
$TS_{(3A\rightarrow4A)}$ + CO_2 + HCOOH	-1639.101313	305.2	21.1	283.6	*85.6* (358.2)
4A + CO_2 + HCOOH	-1639.229491	307.3	21.7	256.1	*7.2* (30.1)

Table S2: Electronic energies, Zero-Point Vibrational Energies, Thermal Energies, Entropies and relative free energies for species calculated at B3LYP\LANL2DZ. for structures described in Figures 4 and 8. Italicized relative free energy values are in kcal mol^{-1} while values in parentheses are in kJ mol^{-1}.

Structure	Electronic energy (Hartrees)	ZPE (kcal mol^{-1})	$\mathbf{H^o_{298} - H^o_0}$ (kcal mol^{-1})	Entropy (cal mol^{-1} K^{-1})	Relative free energy at 298 K
1A	-1639.2886242	312.6	19.6	196.8	*0.0* (0.0)
$TS_{(1A\rightarrow1D)}$	-1639.2696380	312.8	19.8	200.6	*11.1* (46.4)
1D	-1639.2817215	312.8	20.0	202.8	*3.1* (13.0)
$TS_{(1D\rightarrow1E)}$	-1639.2682464	311.8	19.8	199.7	*11.3* (47.3)
1E	-1639.285837	312.6	19.8	199.3	*1.1* (4.6)
$TS_{(1E\rightarrow2C)}$	-1639.1570269	307.9	20.5	208.7	*75.2* (314.6)
2C	-1639.2923679	311.7	21.1	221.7	*-9.2* (-38.5)
2B + CO_2	-1639.288777	312.0	20.5	235.1	*-11.3* (-47.3)
$TS_{(2B\rightarrow3A)}$ + CO_2	-1639.232367	309.8	20.6	241.0	*20.3* (84.9)
3A + CO_2	-1639.262436	310.4	20.9	244.4	*1.3* (5.4)
$TS_{(3A\rightarrow4A)}$ + CO_2 + HCOOH	-1639.101313	305.2	21.1	283.6	*85.6* (358.2)
4A + CO_2 + HCOOH	-1639.229491	307.3	21.7	256.1	*7.2* (-30.1)

Table S3: Electronic energies, Zero-Point Vibrational Energies, Thermal Energies, Entropies and relative free energies for species calculated at B3LYP\LANL2DZ for structures described in Figures 5 and 9. Italicized relative free energy values are in kcal mol^{-1} while values in parentheses are in kJ mol^{-1}.

Structure	Electronic energy (Hartrees)	ZPE (kcal mol^{-1})	$H^{o}_{298} - H^{o}_{0}$ (kcal mol^{-1})	Entropy (cal mol^{-1} K^{-1})	Relative free energy at 298 K (kcal mol^{-1})
1A	-1639.2886242	312.6	19.6	196.8	*0.0* (0.0)
TS$_{(1A\rightarrow1D)}$	-1639.2696380	312.8	19.8	200.6	*11.1* (46.4)
1D	-1639.2817215	311.3	20.0	202.8	*3.1* (13.0)
TS$_{(1D\rightarrow1F)}$	-1639.2355338	312.4	19.9	201.9	*31.9* (133.5)
1F	-1639.250696	312.3	20.2	203.2	*22.1* (92.5)
TS$_{(1F\rightarrow1G)}$	-1639.2404708	311.4	19.9	200.6	*28.1* (117.6)
1G	-1639.259443	314.5	19.2	199.2	*18.1* (75.7)
TS$_{(1G\rightarrow3B)}$	-1639.253522	310.8	20.2	197.7	*19.3* (80.8)
3B	-1639.2720841	313.2	20.0	201.0	*10.1* (42.3)
TS$_{(3B\rightarrow4A)}$ + HOC_2O_2OH	-1639.0980300	307.6	20.3	248.1	*99.8* (417.6)
4A + HOC_2O_2OH	-1639.2268208	309.6	20.9	250.6	*21.4* (89.5)

Table S4: Electronic energies, Zero-Point Vibrational Energies, Thermal Energies, Entropies and relative free energies for species calculated at B3LYP\LANL2DZ for structures shown in Figure 6. Italicized relative free energy values are in kcal mol^{-1} while values in parentheses are in kJ mol^{-1}.

Structure	Electronic energy (Hartrees)	ZPE (kcal mol^{-1})	$\mathbf{H^o_{298} - H^o_0}$ (kcal mol^{-1})	Entropy (cal mol^{-1} K^{-1})	Relative free energy at 298 K
1A	-1639.2886242	312.6	19.6	196.8	*0.0* (0.0)
$TS_{(1A\rightarrow 1D)}$	-1639.2696380	312.8	19.8	200.6	*11.1* (46.4)
1D	-1639.2817215	311.3	20.0	202.8	*3.1* (13.0)
$TS_{(1D\rightarrow OxPtH)}$ + Carnosine	-1639.2181703	311.7	19.9	201.9	*42.0* (175.7)
$TS_{(1D\rightarrow Car)}$ + OxPt	-1639.1995789	310.5	19.8	201.5	*52.5* (219.7)
OxPtH + Car	-1639.2368711	312.7	20.3	207.3	*30.0* (125.5)
Car + OxPtH	-1639.2798599	313.6	19.2	201.1	*5.4* (22.6)